*C*s

Olfactory Perireceptor and Receptor Events in Moths: A Kinetic Model

Karl-Ernst Kaissling

Max-Planck-Institut fuer Verhaltensphysiologie Seewiesen, 82319 Starnberg, Germany

Correspondence to be sent to: Dr Karl-Ernst Kaissling, apl. Prof., Max-Planck-Institut fuer Verhaltensphysiologie Seewiesen, D-82319 Starnberg, Germany. E-mail: Kaissling@mpi-seewiesen.mpg.de

Abstract

A mathematical model of perireceptor and receptor events has been developed for olfactory sensilla on the antennae of the moth *Antheraea polyphemus*. The model includes the adsorptive uptake of pheromone molecules by the olfactory hair, their transport on and within the hair by diffusion, the formation of a complex of pheromone and the extracellular pheromone-binding protein (PBP), the interaction of the complex pheromone–PBP with the hypothetical receptor molecule on the plasma membrane of the olfactory cell, the deactivation of the pheromone and, finally, its enzymatic degradation. In the model the PBP with its reduced form (with one or two intramolecular disulfide bonds) first acts as a carrier of the odorant. Later, while the pheromone is bound, it changes to an oxidized form (three disulfide bonds) with a scavenger function (carrier-to-scavenger model). This process of pheromone deactivation rather than the enzymatic pheromone degradation is responsible for the fall of the receptor potential after stimulus offset. The model is based on morphometrical, radiometrical, electrophysiological and biochemical data reported by several authors. The study supports the idea that peripheral events rather than intracellular signalling processes govern the kinetics of the receptor potential in the unadapted receptor cell.

Introduction

Before pheromone molecules (F) reach the olfactory receptor neuron of an insect antennal hair (sensillum trichodeum), they may interact not only with receptor molecules (R) at the plasma membrane of the neuron but also with various proteins dissolved in the sensillum lymph: the well known pheromone-binding proteins (PBP), and the pheromone-degrading enzymes (E). As suggested in this paper, a further enzyme (N) is involved in the rapid pheromone deactivation postulated by Kaissling (Kaissling, 1972). All of these interactions, the so-called perireceptor events (Getchell *et al.*, 1984; Pelosi, 1996; Hildebrand and Shepherd, 1997; Stengl *et al.*, 1999) and the interactions of stimulus and receptor molecules contribute to olfactory transduction. It will be shown that peripheral interactions rather than intracellular signalling processes may determine the kinetics of the unadapted receptor potential, that is here the change of the transepithelial potential recorded from single sensilla upon pheromone stimulation (Kaissling and Thorson, 1980; Boeckh and Ernst, 1987), as also reflected in the electroantennogram (Schneider, 1992). This idea is based on the observation that receptor potentials elicited by certain pheromone derivatives differ in their kinetics from the responses to the pheromone itself (Kaissling, 1974, 1977, 1998a). In principle, each of the peripheral interactions may contribute to the relationships between the structure of the stimulus molecule and the receptor cell response.

Since Kasang (Kasang, 1971) detected the enzymatic pheromone degradation on the antennae of silkmoths, a mass of experimental data on peripheral interactions has been accumulated which requires a mathematical model for an appropriate interpretation. The data were obtained by using morphometrical (Gnatzy *et al.*, 1984; Keil, 1984), radiometrical (Kanaujia and Kaissling, 1985; Kasang *et al.*, 1988, 1989a,b; Kaissling, 1995), electrophysiological (Zack, 1979; Meng *et al.*, 1989) and biochemical methods (Vogt and Riddiford, 1981, 1986; Vogt *et al.*, 1985; Raming *et al.*, 1989; Du and Prestwich, 1995; Maida *et al.*, 1995, 2000; Ziegelberger, 1995; Prestwich, 1996; Sandler *et al.*, 2000). The analysis is restricted mainly to experiments on the male saturniid moth *Antheraea polyphemus* and the receptor cell responding to the major pheromone component (*E,Z*)-6,11-hexadecadienyl acetate. Some data obtained from *Bombyx mori* are included (Kaissling, 1987) (also A.V. Minor *et al.*, unpublished data).

Several qualitative models of peripheral interactions have been proposed, especially after Vogt and Riddiford (Vogt and Riddiford, 1981) detected the abundant pheromone-binding protein or PBP (Vogt *et al.*, 1999) and the pheromone-degrading enzyme in the sensillum lymph bathing the receptor-cell dendrites inside the hairs. On the basis of morphological contacts between pore tubule and receptor-cell membrane Steinbrecht and Mueller (Steinbrecht and Mueller, 1971), Vogt and Riddiford (Vogt and Riddiford,

1981), and Kaissling (Kaissling, 1986) discussed that the pheromone molecules reach the receptor cell membrane directly via the pore tubule of the hair wall and are, after their excitatory action, deactivated by binding to the PBP. Thus, the binding protein would act as a scavenger. However, the contacts between pore tubules and receptor-cell membrane were observed rarely and their existence turned out to be difficult to prove (Steinbrecht, 1973, 1997; Keil, 1984; Keil and Steinbrecht, 1984). The pheromone-binding assay of Kaissling et al. (Kaissling et al., 1985) demonstrated a solubilizer function of the PBP. Hence the PBP came to be considered as a carrier for the transport of the lipophilic pheromone through the sensillum lymph towards the receptor cell (Vogt et al., 1985; Vogt and Riddiford, 1986). Wojtasek and Leal (Wojtasek and Leal, 1999) and Sandler et al. (Sandler et al., 2000) considered the PBP as a carrier but not a scavenger.

With the PBP as a carrier the mechanism of the rapid pheromone deactivation by binding to the PBP became questionable, since a scavenger would be inappropriate as a carrier. The rapid deactivation had been postulated by Kaissling (Kaissling, 1972) because the enzymatic degradation of the pheromone on the moth antenna *in vivo* takes minutes (Kasang, 1971; Kasang and Kaissling, 1972; Kasang et al., 1988, 1989a,b) and is too slow to account for the fall of the receptor potential within seconds after the end of stimulus exposure. In view of the slow pheromone degradation found *in vivo*, the purified pheromone degrading esterase isolated from *A. polyphemus* antennae acted surprisingly fast (Vogt et al., 1985). This discrepancy would be resolved if the pheromone is protected from degradation while bound to the PBP (Vogt and Riddiford, 1986; Kaissling, 1986, 1987).

Van den Berg and Ziegelberger (Van den Berg and Ziegelberger, 1991) found that pheromone-containing buffer applied inside the hair excited the receptor cell ~100-fold more effectively when PBP was added. This result supported the solubilizer and carrier function of the PBP. Furthermore, it was suggested that the pheromone interacts with the receptor molecule while bound to the PBP (Kaissling, 1986, 1987). The latter view was shared by Du and Prestwich (Du and Prestwich, 1995) and Prestwich (Prestwich, 1996), who studied the binding of pheromone and PBP.

Ziegelberger (Ziegelberger, 1995) presented evidence for the idea that the PBP—sequentially—acts as both a carrier and a scavenger. She found that the PBP does indeed occur in two forms in *A. polyphemus*, a reduced form with one or two disulfide bridges and an oxidized form with three disulfide bridges. Her *in vitro* experiments suggest that pheromone molecules (F) entering the olfactory hair lumen are mostly bound to the PBP in its reduced form (B_{red}), thus being solubilized and transported to the receptor cell. The complex of pheromone and reduced PBP (FB_{red}) may interact with a receptor molecule. Finally it turns into the oxidized form (FB_{ox}), which is assumed to be unable to activate receptor molecules. This 'redox shift' was *in vitro* shown to be catalysed by an agent contained within the olfactory hairs (Ziegelberger, 1995), possibly by the receptor molecules (Kaissling, 1998b; Rospars et al., 2000) or a separate enzyme (N) as discussed by Kaissling (Kaissling, 1998a).

Kaissling (Kaissling, 1998b) quantitatively modeled a simplified reaction scheme, which included the stimulus uptake, the interaction of the stimulatory complex (FB_{red}) and the receptor molecule (R), as well as a pheromone deactivation by the redox shift of the PBP. This model was used to derive tentative rate constants for these reactions. The extended model presented here is based on new experiments and includes further interactions: diffusional transport of the pheromone from the hair surface to the receptor cell; activation of the receptor molecules; binding of pheromone to the PBP; deactivation of the pheromone by the postulated enzyme N; and the enzymatic pheromone degradation. It permits a number of open questions to be discussed on a quantitative basis.

A network of chemical reactions between the stimulus molecule and all of the above reaction partners (R, B_{red}, B_{ox}, E and N) is modeled using a computer program that allows adjustment of the initial concentrations (indicated by $_{(0)}$) of each reaction partner as well as the rate constants for every reaction included. The computer model (see Computer Modeling) simulates the time course of every reaction partner and of the receptor potential elicited by pheromone stimuli of defined intensity and duration.

For comparison and discussion, a simpler model with only one form of the PBP, i.e. without a redox shift, is presented in Appendix B. In this model the free pheromone rather than that bound to PBP interacts with the receptor molecule.

The model reaction network

In the reaction network proposed (Figure 1) the pheromone is adsorbed (reaction 1) and diffuses along the hair surface and through the hair wall via the pore tubules. Entering the hair lumen, the pheromone (F) encounters three reaction partners dissolved in the sensillum lymph: the pheromone-binding protein (PBP), more precisely its reduced (B_{red}) and its oxidized form (B_{ox}), and the pheromone-degrading enzyme (E) (reactions 2, 7 and 8, respectively). The complex FB_{red} interacts with the receptor molecule (R) (reaction 3) whereas the free pheromone (F) and the complex FB_{ox} (and also FE) are unable to activate receptor molecules. The ternary complex ($FB_{red}R$) may go to an activated state ($FB_{red}R'$) which initiates cell excitation (reaction 4). The enzyme (N) postulated here catalyses the redox shift $FB_{red} \rightarrow FB_{ox}$ deactivating the pheromone (reactions 5 and 6). The free pheromone is degraded by the enzyme E (reaction 9). After an initial network of these nine reactions had been constructed, it turned out that further reactions
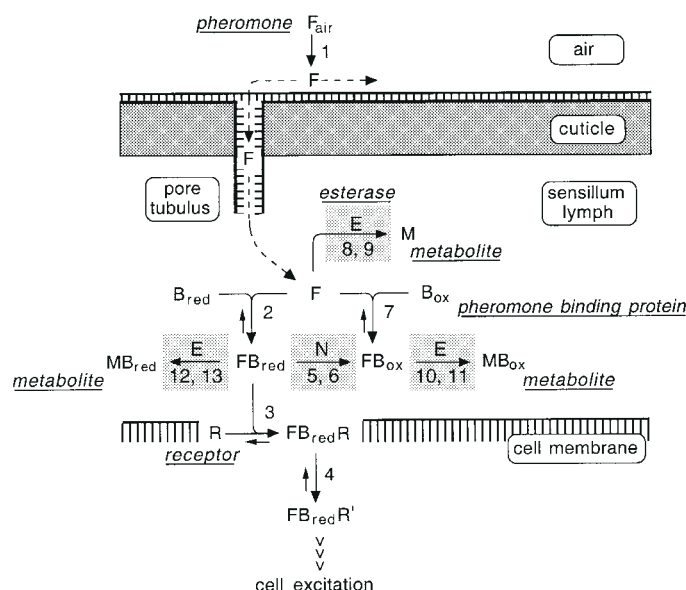
Figure 1   Redox model: hypothetical reaction network of perireceptor and receptor events for pheromone reception in the moth *A. polyphemus*. **(1)** Adsorption of the pheromone F on the surface of the olfactory hair and diffusion towards the receptor cell. **(2)** Binding of F and the reduced form of the binding protein B_{red}. **(3)** Binding of the stimulatory complex FB_{red} to the receptor molecule R at the receptor cell membrane. **(4)** Activation of the ternary complex $FB_{red}R$. The activated complex $FB_{red}R'$ is thought to trigger cellular transduction processes. **(5, 6)** Redox shift of the complex FB_{red} to FB_{ox}, which is catalysed by the postulated enzyme N (pheromone deactivation). **(7)** Binding of F and B_{ox}. **(8, 9)** Enzymatic degradation of F into the metabolite M by the sensillar esterase E. **(10–13)** Degradation of the complexes FB_{ox} and FB_{red} by E into MB_{ox} and MB_{red}, respectively. Small arrows indicate reverse reactions. Areas in grey: enzymatic reactions including association with and dissociation from the enzymes (reactions 5, 8, 10 and 12), and the catalytic reactions 6, 9, 11 and 13 considered to be irreversible.

are required to allow for an enzymatic degradation of the bound pheromone: 10 and 11 for the complex FB_{ox}, or 12 and 13 for FB_{red}. Most reactions can take place in a forward and in a reverse direction, with the rate constants k_i and k_{-i}, respectively. The catalytic steps 6, 9, 11 and 13 of the enzymatic reactions are considered to be irreversible.

Reaction 1: uptake of pheromone by the olfactory hairs

The number of stimulus molecules adsorbed on the antenna of male *A. polyphemus* has been determined for various stimulus intensities using ³H-labelled pheromone. The fraction adsorbed on the sensilla trichodea was 80% of that adsorbed on the whole antenna. At least half of the molecules adsorbed by the hairs were found in the sensillum lymph, and probably most enter the hair lumen (Kanaujia and Kaissling, 1985; Kaissling, 1995). Since very little desorption was found after fresh air had been blown over the antenna for as long as 30 min (Kanaujia and Kaissling, 1985), the amount of stimulus molecules on the antenna must increase linearly during exposure to a constant stimulus flux (Kaissling, 1998a).

Diffusion within the olfactory hair

The latency of single elementary receptor potentials (ERPs, see below) elicited by single pheromone molecules has been thought to be due to diffusion of the pheromone from the adsorption site on the hair surface to the receptor cell dendrite inside the hair lumen. From the latencies—on the average several 100 ms (Kaissling, 1987)—an apparent diffusion coefficient of $5 \cdot 10^{-9}$ cm²/s has been calculated. However, a much larger diffusion coefficient of $3 \cdot 10^{-7}$ cm²/s has been determined for the longitudinal migration of tritium-labelled pheromone on and within the olfactory hairs of *A. polyphemus* (Kanaujia and Kaissling, 1985); see also Steinbrecht (Steinbrecht, 1973) for *Bombyx mori*. As shown below, other processes than diffusion are responsible for the latencies of the ERPs.

The measured diffusion coefficient of $3 \cdot 10^{-7}$ cm²/s most likely applies to the diffusion of stimulus molecules within the sensillum lymph, while bound to the PBP; a diffusion coefficient in this range is expected for a protein of this size (15 kDa). Apparently, the pheromone adsorbed on the cuticle diffuses even faster: the longitudinal migration of pheromone measured for dried hairs was about threefold faster than in intact hairs (Kanaujia and Kaissling, 1985). Tentatively, this migration is considered to occur by diffusion on the cuticle. The diffusion across the hair wall via the pore tubules is assumed to have a coefficient in the same range as cuticular diffusion (assumption A) since the pore tubules seem to consist of the same material as the outermost layer of the hair cuticle (Steinbrecht, 1997).

With a diffusion coefficient $>3 \cdot 10^{-7}$ cm²/s the pheromone molecules would become distributed on and within the hair (diameter 2–3 μm) within <10 ms. Because this time is short compared with the transients of the receptor potential, it seems adequate to express the amount of each molecular species of the network in relation to the total hair volume (2.6 pl), about half of which is occupied by the hair lumen. Accordingly, the adsorptive stimulus uptake U (Figure 1, reaction 1) is defined as the number of pheromone molecules adsorbed per second by a hair divided by the volume of the hair and will be expressed as μM/s.

In order to study the possible effects of diffusion on the receptor potential, especially on its relatively fast rise after stimulus onset, the chemical network model is combined with the diffusion model of J. Thorson, described elsewhere (Kaissling, 1987). In this model the stimulus molecules are adsorbed on a circular area of the hair surface around each pore with a diameter of 0.5 μm, corresponding to the spacing of pores in the hair wall. The adsorbed molecules randomly walk within this area, being reflected at its boundary and trapped at the pore entrance (diameter 10 nm). Then they diffuse along the pore tubules until they reach the inner end and enter the sensillum lymph. The length of the pore tubules (1 μm used here) represents about the average distance from the hair wall to the receptor cell, although in

A. polyphemus the tubules often are shorter and seldom connect with the receptor cell (Keil, 1984). Using an overestimated tubule length may approximately compensate for the fact that the time needed for the transport from the inner end of the tubules to the receptor cell is neglected here.

Reactions 2 and 7: binding of pheromone to PBP

As shown for homogenates of isolated hairs after native gel electrophoresis, B_{red} and B_{ox} comprised 87 and 13% of the PBP, respectively (Ziegelberger, 1995). According to these percentages and to the concentration of the PBP found in the sensillum lymph—5–10 mM (Vogt and Riddiford, 1981; Klein, 1987)—we use initial concentrations (amounts related to the entire hair volume, see above) of 3.5 and 0.5 mM for $B_{red(0)}$ and $B_{ox(0)}$, respectively.

The free pheromone F adsorbed by the hair binds in the model to both forms of the PBP, the reduced form B_{red} (reaction 2) and the oxidized form B_{ox} (reaction 7). After an incubation of the homogenate for 1 min, B_{red} bound 83% and B_{ox} bound 17% of the radiolabelled pheromone component (*E*,*Z*)-6,11-hexadecadienyl acetate (Ziegelberger, 1995). These numbers together with the relative amounts of the two forms of the PBP indicate a similar affinity of the pheromone to either form. Thus, for both forms of the PBP we use the same dissociation constant of 60 nM as determined in a binding assay with the native PBP isolated from antennal branches of *A. polyphemus* (Kaissling *et al*., 1985). The two constants are K_{d2} for FB_{red} [see equation (A16) in Appendix A] and K_{d7} for FB_{ox} [see (A20)]. Using a different assay, Du and Prestwich (Du and Prestwich, 1995) found a K_d of 640 nM for the recombinant PBP, that most likely occurs in the oxidized form. A lower affinity of the oxidized form is supported by recent work (Maida *et al*., 2000). As shown below, the values of the dissociation constants are less important for the model than those of certain rate constants.

Reaction 3: the binding of the stimulatory complex FB$_{red}$ to the receptor molecule

On the basis of the experiments of Van den Berg and Ziegelberger (Van den Berg and Ziegelberger, 1991)—see Introduction—it is assumed that the complex FB_{red} rather than the free pheromone binds to the (for *A. polyphemus* still hypothetical) receptor molecules (assumption B). This assumption seems reasonable if an extremely small fraction of the pheromone in the sensillum lymph is free, i.e. not bound to the PBP, which is expected from the high concentration of the PBP and its dissociation constant (see below).

Reaction 4: the activation of receptors

It is generally assumed that receptor molecules may adopt an activated state due to binding of a ligand (Del Castillo and Katz, 1957; Kaissling, 1977; Lauffenburger and Linderman, 1993; Rospars *et al*., 2000). Accordingly, after binding of

the stimulatory ligand FB_{red} to R we let the complex $FB_{red}R$ change to an activated state $FB_{red}R'$ (reaction 4), which initiates cellular transduction processes. We assume that the activation of the receptor molecules is reflected by the ERPs (assumption C) elicited by single pheromone molecules (Kaissling and Thorson, 1980; Kaissling, 1994a). From the ERPs, rate constants of the receptor activation can be deduced—see below (A.V. Minor *et al*., unpublished data).

Reactions 5 and 6: the redox shift of the PBP

The model includes the assumption that the complex FB_{ox} is inactive; only the complex FB_{red} activates the receptors (assumption D). Accordingly, the redox shift from FB_{red} to FB_{ox} deactivates the pheromone. The redox shift of the PBP found by Ziegelberger (Ziegelberger, 1995) in homogenates of isolated olfactory hairs must be catalysed by an agent within the hair, since no redox shift occurred with purified PBP and pheromone. Here we postulate the existence of an enzyme N catalysing the redox shift (see Discussion).

Reactions 8–13: the enzymatic pheromone degradation

Reactions 8 (association with and dissociation from the enzyme) and 9 (catalytic step) represent the enzymatic degradation of the free pheromone into a non-stimulatory metabolite M. The enzyme concentration *in situ* was estimated as maximally 1/10 000 of the concentration of the pheromone-binding protein (Vogt *et al*., 1985), which amounts to $E_{(0)} = 400$ nM for the model.

Pheromone molecules bound to PBP are largely protected from degradation by the enzyme E (assumption E). This assumption is inferred from experiments of Vogt and Riddiford (Vogt and Riddiford, 1986), who found that PBP added to a solution of pheromone and sensillar esterase, the latter purified from male antennae of *A. polyphemus*, reduced the velocity of pheromone degradation. As shown below, the degradation of only the free pheromone would be much too slow to explain the rate of pheromone degradation measured on intact antennae. This means that the protection cannot be complete; the enzyme must be able to degrade, to some extent, the pheromone bound to PBP (reactions 10–13).

In summary, together with experimental data the following assumptions (A)–(E) were used to construct the reaction network proposed here (Figure 1).

(A)   The transport of pheromone towards the receptor cell occurs with the same diffusion coefficient as determined for longitudinal migration on the hair.

(B)   Only the complex FB_{red} activates the receptor molecules.

(C)   The elementary receptor potentials elicited by single pheromone molecules reflect the temporal pattern of the activation of single receptor molecules.

(D)   The observed redox shift $FB_{red} \rightarrow FB_{ox}$ deactivates the pheromone molecules.

	k_i (forward)	k_{-i} (reverse)	
k_2	0.17/(s·µM)	0.01/s	K_{d2} = 60 nM
k_3	0.209/(s·µM)	7.9/s*	K_{d3} = 37.7 µM
k_4	16.8/s*	98/s*	K_4 = 5.8
k_5	4/(s·µM)	98.9/s	} $K_{m5,6}$ = 32.1 µM
k_6	29.7/s	-·-	
k_7	0.000,17/(s·µM)	0.000,01/s	K_{d7} = 60 nM
k_8	150/(s·µM)	300/s	} $K_{m8,9}$ = 2.2 µM
k_9	30/s	-·-	
k_{10}	0.15/(s·µM)	300/s	} $K_{m10,11}$ = 2.2 mM
k_{11}	30/s	-·-	
k_{12}	0.15/(s·µM)	300/s	} $K_{m12,13}$ = 2.2 mM
k_{13}	30/s	-·-	

$R_{(0)}$ = 1.64 µM $B_{red(0)}$ = 3.5 mM $B_{ox(0)}$ = 0.5 mM

$E_{(0)}$ = 400 nM $N_{(0)}$ = 1 µM

Figure 2 Parameters of the redox model (Figure 1), obtained from biochemical, morphometrical, radiometrical and electrophysiological studies of various authors on *A. polyphemus*, including assumptions and model considerations. Asterisks denote values obtained from *Bombyx mori* (see text). Areas in grey: rate constants of enzymatic reactions.

(E) Pheromone molecules bound to PBP are largely, but not fully protected from enzymatic degradation.

The determination of model parameters

After the construction of a reaction network, tentative model parameters (Figure 2) will be determined analytically, based on experimental data and further assumptions (F) and (G), as shown in the following. In a later section these parameters will be used in a computer simulation of the receptor potential (derived by J. Thorson, Oxford).

The reaction network is described by equations (A1)–(A11) in Appendix A. Some of these equations can be simplified since certain mass flows turned out to be very small in relation to other flows. Thus we obtain the approximate equations (A12)–(A14) from (A1), (A4) and (A8), respectively. Correspondingly, some of the constants for flow equilibrium at constant stimulus uptake U [(A16)–(A23)] are approximate equations [(A16), (A19) and (A20)]. The initial concentrations of E, R and N are given by equations (A24)–(A28). Equation (A24) is simplified to (A25). For saturating stimuli, equation (A26) becomes (A27). The factors Q_1–Q_5, determined experimentally, are defined in equations (A29)–(A33), respectively.

The rate constants for binding of pheromone to PBP (reactions 2 and 7)

For determining the rate constant k_2 we use the flow equilibrium with equation (A15)

$$U = k_2 \cdot F \cdot B_{red} + k_9 \cdot FE \quad (1)$$

Here the very small direct flows of F to and from B_{ox} are neglected (see below). To estimate k_2, we assume that only very few of the stimulus molecules adsorbed are enzymatically degraded before they have a chance to bind to B_{red} and to hit a receptor molecule. Most likely, not only the size and construction of the antenna but also the perireceptor processes in the pheromone sensilla are optimized for providing high sensitivity of pheromone detection. Thus most of the molecules adsorbed, the fraction Q_1 [= 99%, equation (A29)], should bind to B_{red}. Using equations (A21) and (A29) we find from equation (1)

$$\frac{k_2 \cdot F \cdot B_{red}}{Q_1} \approx k_2 \cdot F \cdot B_{red} + \frac{k_9 \cdot E \cdot F}{K_{m8,9}} \quad (2)$$

For small uptake values we set $E \approx E_{(0)}$ and $B_{red} \approx B_{red(0)}$ and find

$$k_2 \approx \frac{k_9 \cdot E_{(0)}}{K_{m8,9} \cdot B_{red(0)} \cdot \left(\dfrac{1}{Q_1} - 1\right)} \quad (3)$$

The K_m of the purified esterase [$K_{m8,9}$ = 2.2 µM, see equation (A21)] and the rate constant k_9 of metabolite production were determined *in vitro* by Vogt *et al*. (Vogt *et al*., 1985). Here we use k_9 = 30/s, which is a value between that derived from Vogt *et al*. (= 45/s) and that from Vogt and Riddiford [= 7/s (Vogt and Riddiford, 1986)]. With a concentration of $E_{(0)}$ = 0.4 µM (Vogt *et al*., 1985), $B_{red(0)}$ = 3.5 mM (see above) and Q_1 = 0.99 we obtain k_2 = 0.154/(µM · s). From this value of k_2 and the dissociation constant K_{d2} = 60 nM [see (A16)] we find k_{-2} = 0.00924/s. In the following we use a rounded value of k_{-2} = 0.01/s and k_2 = 0.17/(µM · s).

For the dissociation of FB_{ox} we choose a rate constant k_{-7} = 0.000,01/s, 1000-fold smaller than k_{-2}, in order to adjust the level of tailing of the receptor potential (see below). From this number and the dissociation constant K_{d7} = 60 nM we arrive at k_7 = 0.000,17/(µM · s) for the association of F and B_{ox}. Note that with this number and with $B_{ox(0)}$ = 0.5 mM (see above), the direct flow of F to B_{ox} (= $k_7 \cdot B_{ox(0)} \cdot F$) is negligible, it amounts to only 1/7000 of the flow of F to B_{red} (= $k_2 \cdot B_{red(0)} \cdot F$).

The rate constants for the receptor interactions (reactions 3 and 4)

On the basis of the assumption C, three rate constants for the interaction of the stimulatory complex FB_{red} with the receptor molecules R have been determined by an analysis of the ERPs (A.V. Minor *et al*., unpublished data). This analysis was done using ERPs recorded extracellularly from pheromone receptor cells of the silkmoth *Bombyx mori*

(Kaissling, 1977, 1994a). The ERPs consist of transient voltage changes (bumps) of small amplitude (<1 mV) and ~10 ms duration which occur as single events or in bursts of two to about ten bumps. It is assumed that a bump reflects a single activation of the receptor molecule, leading to a transient increase of the conductance of the receptor cell membrane; a single pheromone molecule elicits a single activation or a burst of activations when bound to a single receptor molecule (A.V. Minor *et al.*, unpublished data). The measured values included the durations of bumps and the gaps between bumps within the bursts, as well as the number of bumps per burst. From these data several rate constants were calculated: k_{-3} (= 7.9/s) for the dissociation of the ternary complex ($FB_{red}R$), and both rate constants of the activation of the receptor molecule, k_4 (= 16.8/s) and k_{-4} (= 98/s). These rate constants are considered as tentative values for the model discussed here for *A. polyphemus*. The rate constant k_3 was determined from the response kinetics as shown below.

The receptor molecules (R) and the postulated enzyme (N) (reactions 3, 5 and 6)

The model parameters $R_{(0)}$, k_3, and two of the parameters $N_{(0)}$, k_5, k_{-5} and k_6 may be determined from experimental data, i.e. from:

- the stimulus uptake U_{sat} necessary for the saturation of the receptor potential amplitude;
- the rate constant k_{fall} of the fall of $FB_{red}R'$ after stimulus offset, obtained from the fall of the receptor potential; and
- the fraction Q_3 of stimulus molecules adsorbed at weak stimulation which elicit elementary responses.

(1) For a flux detector at flow equilibrium, U_{sat} is the uptake at which saturation of the receptor molecules is reached (Kaissling, 1998a). U_{sat} can be defined from the uptake–response relationship for $FB_{red}R'$ at flow equilibrium which is derived in Appendix A [equation (A38)]

$$\frac{FB_{red}R'}{FB_{red}R'_{max}} \approx \frac{1}{\frac{K_{d3} \cdot Q_4}{K_{m5,6}} \left(\frac{k_6 \cdot N_{(0)}}{U \cdot Q_1} - 1 \right) + 1} \quad (4)$$

It seems reasonable (see below) to assume that receptor R and enzyme N half-saturate at the same concentration of FB_{red} (assumption F). With this assumption ($K_{d3} \cdot Q_4 = K_{m5,6}$) we find equation (A40)

$$\frac{FB_{red}R'}{FB_{red}R'_{max}} \approx \frac{U \cdot Q_1}{k_6 \cdot N_{(0)}} \quad (5)$$

showing a linear dependence of $FB_{red}R'$ on U. If we set this

equation = 1 for the maximum value of $FB_{red}R'$, we obtain equation (A41)

$$k_6 \cdot N_{(0)} \approx U_{sat} \cdot Q_1 \quad (6)$$

The uptake U_{sat} must be reached at (or above) saturation of the uptake–response curve of the steady receptor potential amplitude. From the measured curve (Figure 3A) we take $U_{sat} = 30 \ \mu M/s$ as a minimum value, and obtain the product $k_6 \cdot N_{(0)} \approx 29.7 \ \mu M/s$.
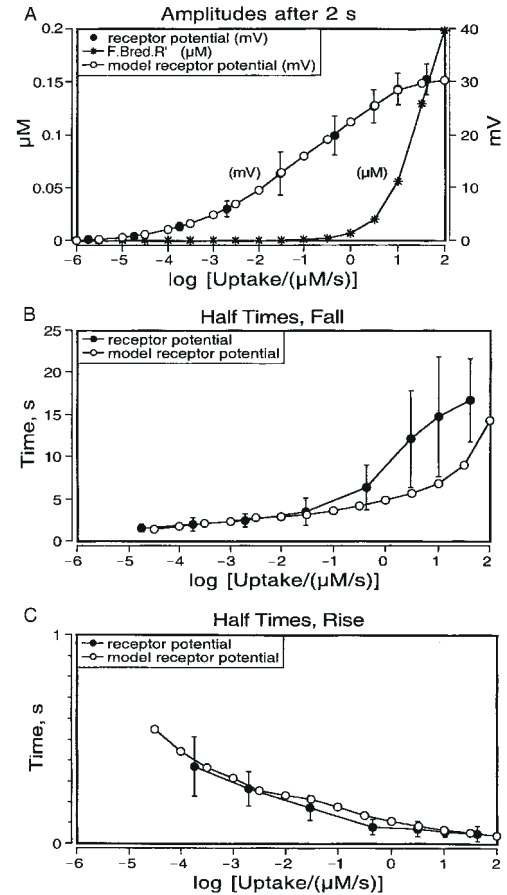

Figure 3 Dose–response functions of the receptor potential recorded (dots), comparison with the redox model (circles). Abscissa: stimulus uptake U (molecules adsorbed per second and per total hair volume, given in $\mu M/s$) calibrated using the ^{3}H-labelled pheromone (Kaissling *et al.*, 1987; Kaissling, 1995). Dots: data obtained from recordings from single sensilla trichodea of male *A. polyphemus* stimulated by the major pheromone component (*E,Z*)-6,11-hexadecadienyl acetate (Zack, 1979). The lower three values were re-measured by Blanka Pophof (Seewiesen). Circles: responses of the redox model using the standard parameters (Figure 2). **(A)** Steady mV-amplitudes of the receptor potential reached after stimulation for 2 s. The steady μM-levels of FBredR' reached after 2 s increase in linear proportion to the uptake, over the entire range of the latter. **(B, C)** Half times of the transients of the receptor potentials after stimulus offset (fall) and onset (rise), respectively. All model amplitudes in (A) and the one model half-time at the 'adjustment uptake' of –2 in (B) were adjusted to the data. All other model half-times in (B) and (C) were obtained after conversion of the FBredR' values into mV amplitudes (see text).

(2) The rate constant k_{fall} of the fall of $FB_{red}R'$ after stimulus offset is

$$k_{fall} = -\frac{dFB_{red}R'}{dt \cdot FB_{red}R'} = -\frac{dFB_{red}R}{dt \cdot FB_{red}R} = -\frac{dFB_{red}}{dt \cdot FB_{red}} \approx +\frac{dFB_{ox}}{dt \cdot FB_{red}}$$

(7)

Using equations (A14) and (A19) for small uptake values we find

$$\frac{dFB_{ox}}{dt \cdot FB_{red}} \approx \frac{k_6 \cdot N_{(0)}}{K_{m5,6}}$$

(8)

Thus we may use k_{fall} in order to determine Q_2 [equation (A30)]

$$k_{fall} = \frac{k_6 \cdot N_{(0)}}{K_{m5,6}} = Q_2$$

(9)

The value of k_{fall} may be estimated using the fall of the receptor potential after stimulus offset. For this purpose, the momentary amplitude of the receptor potential (in mV) has to be converted into the concentration of the activated receptors ($FB_{red}R'$). This conversion is based on the assumption that during the relatively slow fall of the potential after stimulus offset, the relationship between the mV-amplitude and $FB_{red}R'$ at every moment is approximately the same as at flow equilibrium—assumption G (Kaissling, 1998b). The same relationship we find between the mV-amplitude and the uptake U, since at flow equilibrium $FB_{red}R'$ is proportional to U. With assumption F we find this proportionality from equations (5) and (6)

$$FB_{red}R' \approx \frac{FB_{red}R'_{max}}{U_{sat}} \cdot U$$

(10)

For $U_{sat} = 30$ μM/s and $FB_{red}R'_{max} = 0.2$ μM (Figure 3A), the proportionality factor is $FB_{red}R'/U_{sat} = $ s/150.

The relationship between the 'steady' mV-amplitudes of the receptor potential and $FB_{red}R'$ is represented by the 'steady' uptake–response function covering a wide range of antennal stimulus uptake (Figure 3A, dots). The responses were measured by Zack (Zack, 1979) after 2 s of stimulation when the receptor potential almost reached a constant level. The uptake was calibrated by means of radiolabelled pheromone (Kanaujia and Kaissling, 1985; Kaissling, 1995). The empirical uptake–response function was implemented in the computer program (Figure 3A, circles). Asterisks in Figure 3A give the linear increase of $FB_{red}R'$ for 2 s stimuli, in the lower range of uptake not visible in the semilog plot.

By means of the 'steady' uptake–response function and on the basis of assumption G and equation (10) the momentary receptor potential amplitudes during the fall of the receptor potential were converted into momentary values of $FB_{red}R'/FB_{red}R'_{max}$. This way the fall of $FB_{red}R'$ was reconstructed from the fall of the receptor potential after stimulus offset, and from this the half life $t_{fall/2}$ of $FB_{red}R'$ was determined. A value of $t_{fall/2} = 0.83$ s was determined for an 'adjustment uptake' of 0.01 μM/s, in the lower range of uptakes. From the relationship

$$k_{fall} = \ln2/t_{fall/2} \approx Q_2$$

(11)

we find $k_{fall} = 0.83$. For calculating the model parameters we use the approximate value of k_{fall}, namely $Q_2 = 0.924$/s [equation (9)] which reveals optimal simulation of the fall time at the adjustment uptake. From equations (A30) and (6) we find

$$K_{m5,6} \approx \frac{U_{sat} \cdot Q_1}{Q_2} = \frac{30 \cdot 0.99}{0.924} = 32.1 \text{ μM}$$

(12)

According to assumption F and using equation (A32) we find $K_{d3} = 37.7$ μM. With the latter and equation (A17) we obtain $k_3 = 0.209/(μM \cdot s)$.

From $k_6 \cdot N_{(0)} = 29.7$ μM/s and $K_{m5,6} = 32.1$ we may determine possible sets of the partially free parameters $N_{(0)}$, k_5, k_{-5} and k_6, by arbitrarily choosing two of the four parameters. For instance, if we set $N_{(0)} = 1$ μM, we get $k_6 = 29.7$/s, and if we then set $k_5 = 4/(μM \cdot s)$, we get $k_{-5} = K_{m5,6} \cdot k_5 - k_6 = 98.9$/s.

It should be noted that the velocity of the redox shift was measured using homogenates of isolated olfactory hairs (Ziegelberger, 1995; Kaissling, 1998b). Taking into account the 200-fold dilution of the homogenate, the rate constant of the redox shift *in vitro* [determined from Figure 6 in Ziegelberger (Ziegelberger, 1995)] is $k_{fall\ in\ vitro} = 0.074$/s, which is 8% of Q_2, the value of k_{fall} used for optimal simulation (see above). The fact that $k_{fall\ in\ vitro}$ is smaller than k_{fall} could indicate partial decomposition of the enzyme N in the homogenate assuming that the rate constants k_5, k_{-5} and k_6 are unchanged *in vitro*.

(3) For determining $R_{(0)}$ we need the fraction Q_3 [equation (A31)] of pheromone molecules adsorbed by the antenna activating a receptor molecule. Voltage recordings at weak stimulus intensities revealed that 25% of the molecules adsorbed elicited a nerve impulse (Kaissling, 1987). The spikes are preceded by ERPs which are thought to reflect activations of single receptor molecules (see above). Consequently, the rate r_{ERP} of the ERPs [equation (A42)] depends on the rate of associations of FB_{red} and R and on the fraction Q_5 [equation (A33)] of the $FB_{red}R$ complexes formed that become activated. As shown in Appendix A, equations (A42) and (A43) can be used to calculate $R_{(0)}$ [equations (A44)–(A46)]. With assumption F we find equation (A47)

$$R_{(0)} \approx Q_3 \cdot U_{sat} \cdot \left(\frac{1}{k_{-3}} + \frac{1}{k_4} + \frac{1}{k_{-4}} + \frac{k_4}{k_{-3} \cdot k_{-4}} \right) \quad (13)$$

where the expression in brackets (= 0.22 s) can be considered as a dwelling time of the pheromone in the ternary complex ($FB_{red}R$ and $FB_{red}R'$). Since not all ERPs elicit a nerve impulse, $Q_3 = 25\%$ is a minimum value. Also $U_{sat} = 30\ \mu M/s$ is a minimum value (see above). Consequently, $R_{(0)}$ is a minimum value. Using the above values of Q_3 and U_{sat} in equation (13) we find $R_{(0)} \approx 1.6\ \mu M$. This is ~15% of the value of 10.9 μM expected for the maximum density of receptor molecules in the plasma membrane of the receptor cell dendrite, with 40 000 units per μm^2 (see Discussion). Assumption F ($K_{d3} \cdot Q_4 = K_{m5,6}$) seems reasonable since $K_{d3} \cdot Q_4 > K_{m5,6}$ would reveal even higher numbers of receptor molecules, whereas $K_{d3} \cdot Q_4 < K_{m5,6}$ would let the receptors half-saturate at too low uptake values (Kaissling, 1998a).

The rate constants for the enzymatic degradation of the free pheromone F (reactions 8 and 9)

For the dissociation of F and E we set k_{-8} ten times higher than k_9 (= 30/s, determined for the purified esterase by Vogt *et al.*, see above) to $k_{-8} = 300/s$, according to common enzyme systems, in which the product formation is the slowest reaction. From Vogt's value of $K_{m8,9} = 2.2\ \mu M$ and $k_9 = 30/s$ we then obtain $k_8 = 150/(s \cdot \mu M)$.

The rate constants for the degradation of the complexes FB_{ox} and FB_{red} (reactions 10 to 13)

The half life of the pheromone adsorbed on living antennae of male *A. polyphemus* was found to be 3.0 ± 0.3 min (Kasang *et al.*, 1988), whereas the half life obtained from the simulation of the reactions 1–9 is >1000-fold larger. The modeled half life is too long if only the free pheromone is enzymatically degraded (reactions 8 and 9) and since the proportion of free/bound pheromone is small. The small proportion of free pheromone results from the high concentration of the PBP and the high association rate k_2 of PBP and pheromone as demonstrated in the following.

The computer simulation of the reactions 1–9 shows that during and even more after the stimulation offset, the fraction of the free pheromone (F) is minute and most of the pheromone adsorbed is bound to B_{red} and B_{ox}. For instance, with an uptake of 1 $\mu M/s$ we find the following concentrations at the end of a 2 s stimulus

$F = 0.0018\ \mu M$ $FB_{red} = 0.87\ \mu M$ $FB_{ox} = 1.0\ \mu M$
$M = 0.0186\ \mu M$

At 8 s after stimulation offset we have

$F = 5 \cdot 10^{-8}\ \mu M$ $FB_{red} = 0.001\ \mu M$ $FB_{ox} = 1.965\ \mu M$
$M = 0.0187\ \mu M$.

The ratio free/bound is $F/(FB_{red} + FB_{ox}) \approx 10^{-3}$ during, and $\approx 4 \cdot 10^{-7}$ after, stimulation. From the above discrepancy between the half life of the pheromone measured on the antenna and the half life expected from the reactions 1–9 we conclude that the pheromone bound to the PBP is not fully protected from the enzyme. Thus, a limited degradation of the large amount of pheromone bound to PBP must occur. We propose that the enzyme is able to bind and to metabolize the complex FB_{ox} to a non-stimulatory metabolite MB_{ox} (reactions 10 and 11, Figure 1). In order to fit the measured pheromone degradation we set the value of the rate constant k_{10} for the association of FB_{ox} and E 1000-fold smaller than k_8 [$k_{10} = 0.15/(\mu M \cdot s)$] whereas we keep k_{-10} (= 300/s) and k_{11} (= 30/s) equal to k_{-8} and k_9, respectively. This corresponds to an affinity between FB_{ox} and E with $K_{m10,11} = 2.2\ mM$ [equation (A22)], which is 1000-fold smaller than that between F and E (with $K_{m8,9}$).

A high value of $K_{m10,11}$ is supported by observations in living *Bombyx* antennae loaded with high doses of radio-labelled bombykol. The bombykol degradation did not saturate at antennal loads of 10^{13} pheromone molecules, corresponding to a concentration of ~1 mM on the hair (Kasang and Kaissling, 1972). Signs of saturation (prolonged half life of pheromone) were detected when the antennal load was increased to 10^{15} pheromone molecules (Kasang, 1973). We assume similar concentrations of saturating stimuli for *A. polyphemus* since there are similarities in pheromone degradation in the two species. Thus, the half life of pheromone was 3.5 min in male *Bombyx* antennae (Kasang and Kaissling, 1972) and 3 min in male antennae of *A. polyphemus* (Kasang *et al.* 1988). Metabolic pheromone breakdown was found on isolated hairs of *A. polyphemus* (Kasang *et al.*, 1989b).

According to equations (A11a) and (A22), the velocity of degradation of FB_{ox} is given (for $FB_{ox} < K_{m10,11}$) by

$$\frac{dMB_{ox}}{dt} \approx \frac{k_{11} \cdot E_{(0)} \cdot FB_{ox}}{K_{m10,11}} \quad (14)$$

With $K_{m10,11} = 2.2\ mM$ and if the rate constants k_{-10} and k_{11} are kept equal to k_{-8} (= 300/s) and k_9 (= 30/s), respectively, the computer simulation (see below) shows a half life of the bound pheromone FB_{ox} of 2 min, in the range of the measured half life of 3 min (Figure 4). Due to the high value of $K_{m10,11}$, the half life of the pheromone on the antenna is constant up to an uptake of 100 $\mu M/s$.

In summary, in spite of the 1000-fold lower affinity of FB_{ox} and E, compared with that of F and E, most of the pheromone adsorbed on the hair is degraded while bound to B_{ox}—simply because the concentration of FB_{ox} is so much larger than that of F.

Finally, in analogy to the degradation of FB_{ox} we introduce a degradation of FB_{red} (reactions 12 and 13, Figure 1).
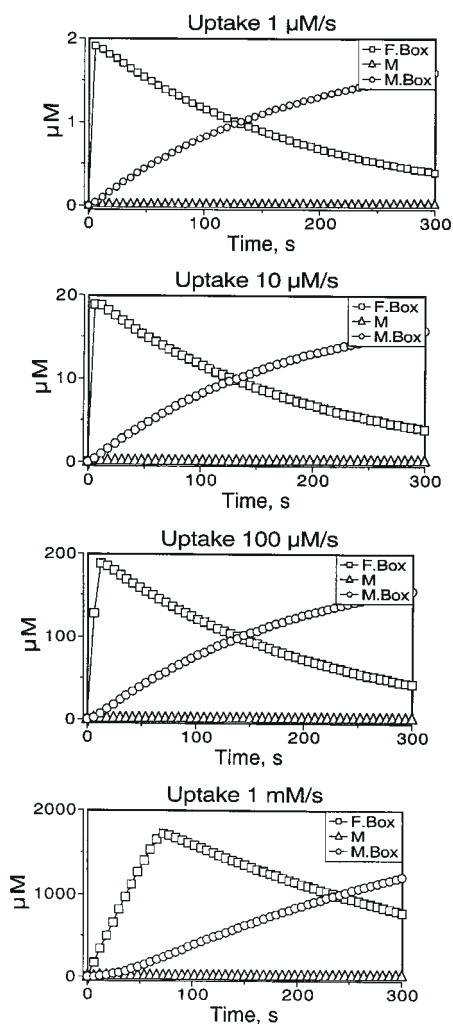
Figure 4 Redox model, pheromone degradation at different loads of pheromone. Stimulus duration 2 s. At lower stimulus loads, half of the pheromone is metabolized after ~2 min (with $k_{10} = 1000\, k_8$). At an uptake of 1 mM/s the enzyme N is near to saturation which slows down the decline of FB_{ox}.

The rate constants are set equal to those of the reactions 10 and 11:

$$k_{12} = k_{10} = 0.15/(s \cdot \mu M),\ k_{-12} = k_{-10} = 300/s\ \text{and}\ k_{13} = k_{11} = 30/s.$$

The simulation of the receptor potential

The time course of the receptor potential was simulated using the model parameters determined above. In a later section the model parameters will be varied in order to demonstrate their influence on the kinetics of the receptor potential.

For a constant stimulus uptake and a given stimulus duration, the computer model first calculates the time course of the concentrations of each molecular species including the active ternary complex $FB_{red}R'$. Examples

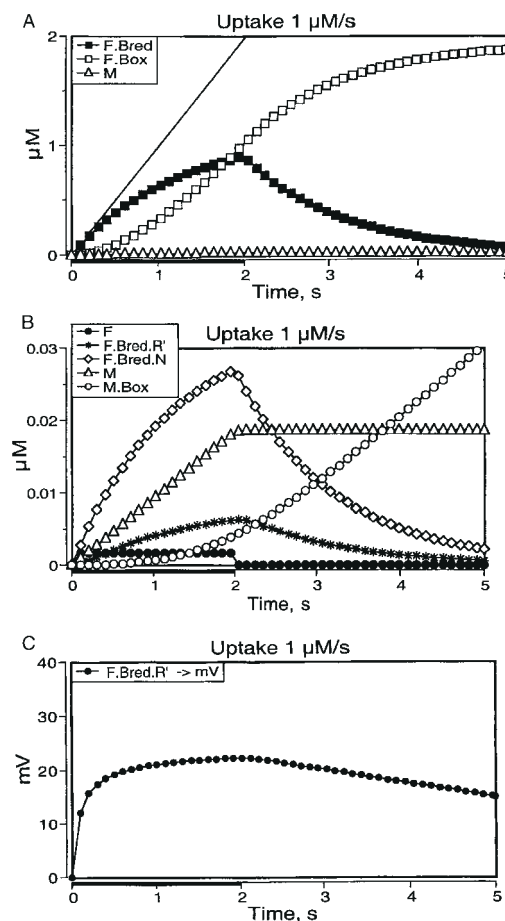**Figure 5** Time course of (redox) model variables after a 2 s stimulus with a medium uptake of 1 µM/s. Model parameters as in Figure 2. Line without symbols in **(A)** shows the product of pheromone uptake and time. The concentration of the free pheromone F shows a most rapid increase and fall **(B)** whereas FB_{red} (A) and $FB_{red}R'$ (B) show much slower transients. The model receptor potential **(C)** shows the typical asymmetrical shape with rapid rise and slow fall, produced by the conversion of $FB_{red}R'$ values into mV amplitudes.

generated using the set of parameters listed in Figure 2 are shown in Figure 5A and B for a medium stimulus uptake (1 µM/s). Then the values of $FB_{red}R'$ during and after stimulation are converted into mV-values (Figure 5C) by means of the uptake–response function as described above.

After implementing the steady uptake–response function (Figure 3A, circles), the computer program generates dose–response curves of the model receptor potential (a) for the half time of its fall after stimulus offset (Figure 3B) and (b) for its rise after stimulus onset (Figure 3C). As described above, the model half life of the fall of the receptor potential was adjusted to the data for an 'adjustment uptake' of 0.01 µM/s. For uptakes below 0.01 µM/s, the simulated model half lives (Figure 3B, circles) agree with the data (Figure 3B, dots). At higher uptakes, however, the model half lives are smaller than those measured. This discrepancy may be due to alterations of intracellular transduction processes at high stimulus intensities (adaptation).

Furthermore, the model almost correctly produces the fast rise times of the receptor potential over the entire range of uptake values (Figure 3C). The good fit of the rise times suggests that the intracellular processes leading from the receptor activation to the electrical signal are fast enough to reflect even the rapid increase of receptor activation upon onset of strong stimuli (see Discussion). It also suggests that adaptation does not occur during the rise. The fit supports assumption G, on which the conversion between mV amplitudes and the concentration of $FB_{red}R'$ was based (see above). In conclusion, the model satisfactorily simulates the transients of the receptor potential, with the exception of the fall times at higher uptake values.

The model offers an explanation for further characteristics of the receptor potential kinetics: saturation effects, the tailing of the response, and the initial delay of the receptor potential seen at strong stimuli. This is demonstrated by simulating the responses of single receptor cells to brief stimuli applied to a single sensillum (Figure 6). For
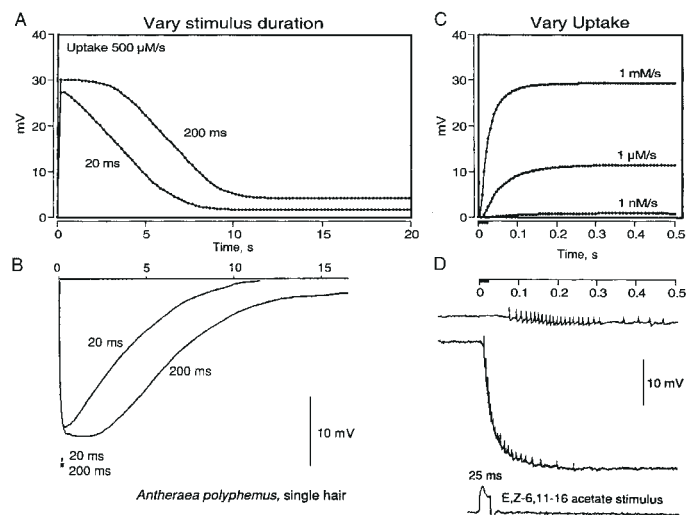

Figure 6 Receptor potentials (= negative deflection of the transepithelial potential) simulated by the redox model **(A, C)** and recorded from single sensilla of *A. polyphemus* **(B, D)**, shown at different time scales. Note that in (B) and (D) the rise of the recorded receptor potentials is plotted downwards, the fall upwards. (A, B) Saturating stimuli of 20 and 200 ms duration. The saturation amplitude of the model receptor potential was adjusted to 31 mV, the maximum average value reported for the major pheromone component (*E,Z*)-6,11-hexadecadienyl acetate (AC1) (Zack, 1979). In (A) the concentration of $N_{(0)}$ was set to 1.8 μM, in order to fit the fall of the recorded potentials. Upon 200 ms stimulation, the fall of the potential starts with a delay of ∼2 s, indicating oversaturation of the system. The model responses show the typical tailing of the receptor potential often observed at high stimulus intensities. An uptake of 1 nM/s resembles 1.6×10^3 molecules per hair (volume 2.6 pl) and per second. (C, D) Rise of receptor potentials at weak and saturating stimuli. The bottom trace in (D) shows the time of stimulus exposure at the olfactory hair (25 ± 1 ms), monitored by a pressure detector. (D) Nerve impulses are superimposed on the receptor potential. Upon strong stimulation impulse firing of the AC1 cell starts after 15 ms, but also the second cell in the hair cell tuned to (*E,Z*)-6,11-hexadecadienal (AL) responds weakly. Its first nerve impulse appears after ∼50 ms (see also Figure 7B).

the simulation of the responses shown in Figure 6A, the concentration $N_{(0)}$ was changed from 1 to 1.8 μM, since the fall of the recorded potentials was somewhat faster than the average fall.

The simulated receptor potentials (Figure 6A,C) agreed satisfactorily with the measured receptor potentials (Figure 6B,D). With an uptake of 500 μM/s for 200 ms, the fall of the receptor potential was delayed by about 2 s after stimulation (Figure 6A,B). This indicates that the response was saturated, as expected above a stimulus uptake $U_{sat} = 30$ μM/s. Furthermore, the fall of the simulated receptor potential (Figure 6A) exhibits the typical tailing as often observed in recorded receptor potentials, especially at high stimulus loads on the antenna—Figure 6B (Kaissling, 1998a). As shown below, the tailing may be explained by the dissociation of the complex FB_{ox}. The initial rise of modeled and recorded receptor potentials is compared in Figure 6C and D. The responses obtained with stimulation of single sensilla at unknown stimulus intensities correspond to model responses at uptake values in the range of 1 nM/s and 1 mM/s, respectively.

Finally, the influence of diffusion on the initial rise of the receptor potential becomes obvious at very strong stimuli (Figure 7A,B). With the diffusion parameters chosen (see above), the rise of the model receptor potential starts after a delay of a few milliseconds (Figure 7A). It fits approximately to the delay observed in single-sensillum recordings at very strong stimuli (Figure 7B). No such delay of the model response is seen if diffusion is made infinitely fast (Figure 7A, smooth curve). These results support assumption A and further strengthen the hypothesis that the extracellular processes govern the kinetics of the receptor potential. Diffusion does not noticeably affect the comparatively slow fall of the receptor potential (not shown).

In summary, the simulation shows that saturation effects, the tailing of the response, and the initial delay of the receptor potential can be produced by perireceptor events rather than intracellular processes. The idea that perireceptor events govern the kinetics of the receptor potential is supported by the observation that saturation effects are obtained with pheromone derivatives, although these compounds elicit smaller maximum amplitudes of the receptor potential (Kaissling, 1972).

Variation of model parameters

By varying the model parameters we examine the influence of rate constants and initial concentrations on the kinetics of the receptor potential. We vary single model parameters by a factor of ten up and down and show the model responses (in mV) to a standard stimulus of a nonsaturating uptake of 1 μM/s and 2 s duration (dots in Figures 8–11). In this section we study the amplitude of the receptor potential and its fall after stimulus offset for the
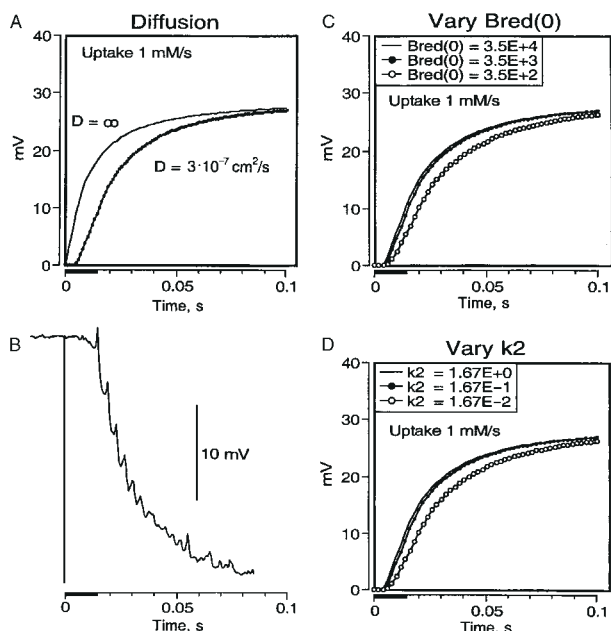
Figure 7 The rise of responses at saturating stimuli. The model receptor potential **(A)** shows an initial delay similar to that of the recorded potential (~10 ms) **(B)**. The delay disappears if diffusion is made infinitely high (A, thinner curve). The model receptor potential rises more slowly if the concentration $B_{(0)}$ or the rate constant k_2 is reduced (C and D, respectively). An increase of the two parameters has almost no effect. Variation of k_{-2} does not affect the rise (see also Figure 9). (B) Nerve impulses are superimposed on the receptor potential. The first nerve impulse of the AL cell appears after ~50 ms (see also Figure 6D).

redox model. For comparisons with the alternative model see Appendix B and Figures A6 and A7.

Varying stimulus intensity (Figure 8A, see also Figure 3A)

Besides amplitude, rise and fall of the receptor potential (Figure 3), the stimulus uptake influences the level of tailing. For the standard set of parameters (Figure 2) and 2 s stimuli we find tailing levels of 0.15, 2, 3, 6.3 and 11.6 mV for uptake values of 0.1, 1, 10, 100 and 1000 µM/s, respectively. For the following comparisons, responses to the standard uptake of 1 µM/s and its variations are shown in Figure 8 (Vary Uptake).

Varying the interaction with the receptor molecules (Figure 8)

Variation of the number of receptor molecules $R_{(0)}$ and of the rate constants k_3 and k_4, has effects like those of varying the stimulus uptake. Reciprocal effects occur upon varying k_{-3} and k_{-4}. The response amplitude is affected and the half time of the fall of the receptor potential changes to a minor extent. A smaller $R_{(0)}$ could be compensated, for instance, by a larger k_3; this would imply a larger affinity between pheromone and receptor.
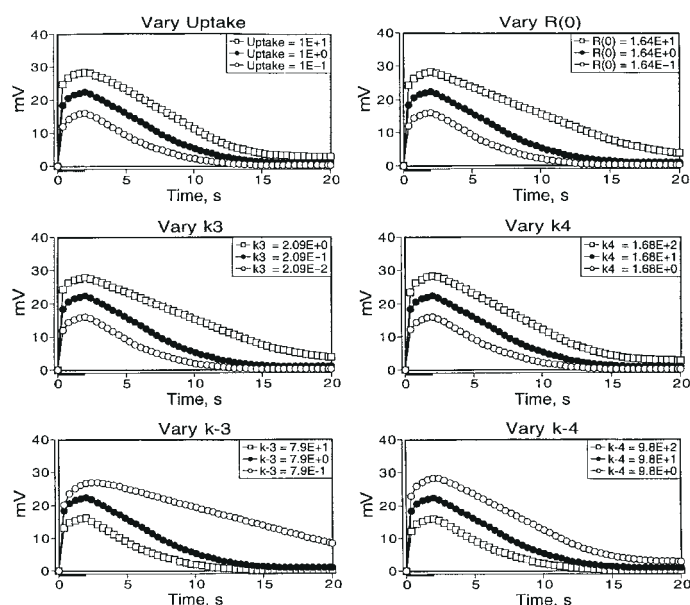

Figure 8 Receptor potentials generated by the redox model upon variation by factors of 10 of the pheromone uptake, the receptor concentration $R_{(0)}$, and the rate constants involved in the receptor interaction (reactions 3 and 4). The standard pheromone uptake (dots) was 1 µM/s, the stimulus duration 2 s. Variations of the concentration of $R_{(0)}$, and of the rate constants, show effects like those produced by the variation of the uptake.

Varying pheromone binding to the PBP (Figure 9)

Changes in the concentration of B_{red} and B_{ox}, as well as variation of the rate constants k_2, k_{-2} and k_7 by a factor of ten up and down, practically do not influence amplitude and fall of the receptor potential. Consequently, within the limits of the factor 10 to 1/10, the values of the dissociation constants K_{d2} and K_{d7} are also of no importance for the responses. Variations of B_{red} and k_2, however, do have clear effects on the rise time of the receptor potential (Figure 7C and D). With ten times smaller B_{red} or k_2 the half time of the rise would increase by 10 ms, or more, depending on stimulus intensity. In addition, the efficiency of pheromone binding to B_{red} represented by Q_1 [equation (A29)] would decrease. In contrast, an increase of k_2 has almost no effect.

Interestingly, k_{-7} strongly determines the level of tailing; a higher level is obtained by a larger k_{-7}, which increases the rate of dissociation of F from the deactivated complex FB_{ox} (Figure 9). The influence of k_{-7} on the tailing is similar in the alternative model (Figure A7). The tailing is abolished if the pheromone is not allowed to dissociate from the complex FB_{ox}, i.e. with $k_7 = 0$, a condition which may be physically improbable. The height of the tailing level in relation to the peak amplitude was adjusted to match that in measured receptor potentials (Figure 6B) by choosing $k_{-7} = 0.000\ 01/s$ (see above).

Varying the redox shift (Figure 10, left-hand panels)

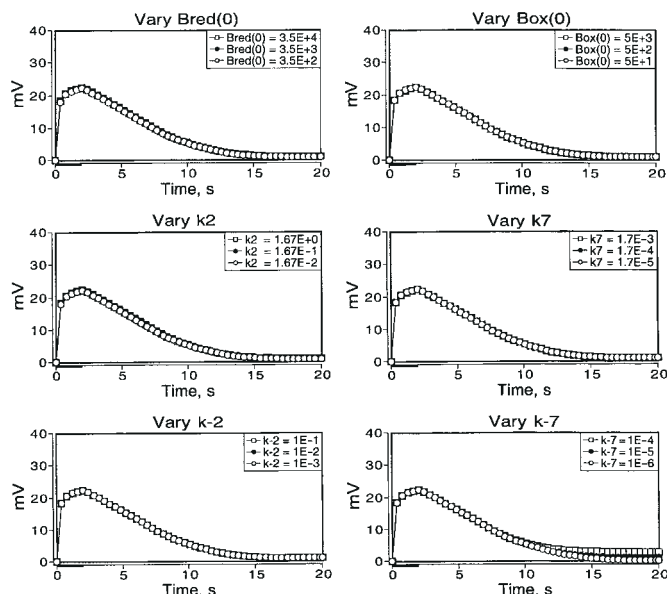The velocity of the redox shift and, consequently, the fall of

Figure 9 Variation of the concentrations of the reduced ($B_{red(0)}$) and the oxidized form ($B_{ox(0)}$) of the PBP, and the rate constants for association (k_2, k_7) and dissociation (k_{-2}, k_{-7}) of the pheromone. These parameters do not influence the fall of the receptor potential, except for k_{-7}, which controls the tailing of the receptor potential. The rise of the receptor potential is affected by k_2 (see Figure 7).
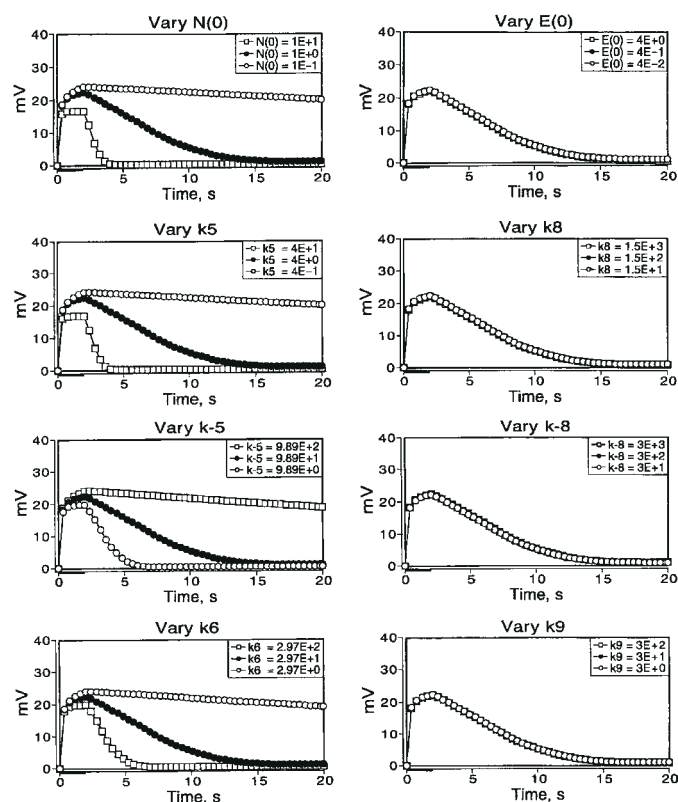

Figure 10 Variation of parameters involved in the redox shift, catalysed by the postulated enzyme N (reactions 5 and 6), and in the degradation of the free pheromone F, catalysed by the sensillar esterase E (reactions 8 and 9). The redox shift has strong effects on the fall of the receptor potential (panels at the left), whereas the enzymatic degradation does not control the response kinetics during the first 20 s after stimulation (panels at the right).
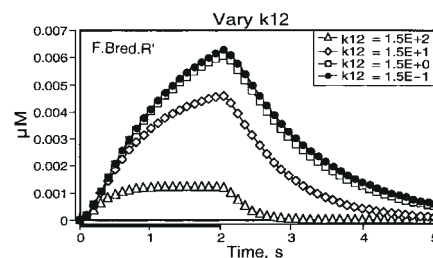
the receptor potential strongly depend on the four, partially free parameters $N_{(0)}$, k_5, k_{-5} and k_6 (Figure 10). The dependence is similar for $N_{(0)}$, k_5 and k_6, and reciprocal for k_{-5}. Effects on the half time of the fall due to altering these parameters are much larger than those obtained by varying $R_{(0)}$, k_3, k_{-3}, k_4 and k_{-4}.

Varying the enzymatic degradation of the free pheromone (Figure 10, right-hand panels)

The enzymatic pheromone degradation in the model has practically no influence on the fall of the receptor potential; its slope remains unchanged even if one completely removes the enzyme. This result is consistent with the observation that the fall is not affected in antennae that happen to have <1% of the regular amount of the sensillar esterase (Maida *et al.*, 1995). The situation differs for the alternative model (see Appendix B and Figure A6).

Varying the protection of the pheromone bound to PBP from enzymatic degradation (Figure 11)

The introduction of reactions 10–13 in the computer model does not noticeably alter the time course of the receptor potential during the first 20 s (not shown). Even if the protection from degradation of pheromone bound to B_{ox} is removed by setting $k_{10} = k_8$, there would be no visible effect on the fall of the receptor potential. However, the tailing would disappear due to the 1000-fold faster degradation of the complex FB_{ox} and the smaller amount of F dissociating

Figure 11 Variation of the protection of the pheromone bound to the reduced form of the PBP. Protection from enzymatic degradation is obtained by decreasing k_{12}, starting from $k_{12} = k_8 = 150/(\mu M \times s)$ (open triangles), that lowers the affinity of FB_{red} and E. The protection increases $FB_{red}R'$ by up to fivefold.

from it (not shown); actually this appears advantageous (see Discussion).

Reducing the protection of F bound to B_{red} by a 10-fold increase of k_{12} to 1.5/($\mu M \cdot$ s) would not change the time course of the receptor potential. However, if k_{12} is further increased, the fall of $FB_{red}R'$ becomes faster. If the protection of F bound to B_{red} is completely removed, i.e. if

$k_{12} = k_8$, the response amplitude is reduced to ~20% (Figure 11). This reduction corresponds to an at least fivefold higher threshold concentration of the pheromone, due to a loss of pheromone molecules (bound to B_{red}) on their way to the receptor molecules.

Varying diffusion

A decrease of the diffusion coefficient by a factor ten would mainly increase the initial delay of the receptor potential; the relatively slow fall of the receptor potential would not noticeably be affected. Details of diffusion will be treated in a separate paper.

Discussion

The proposed network model of perireceptor and receptor events (here called redox model) satisfactorily simulates the receptor potential kinetics of an unadapted receptor cell. Before discussing this model we ask whether a simulation is possible with a simpler model network, which is related to earlier, qualitative models (Vogt and Riddiford, 1981, 1986; Vogt et al., 1985, 1987). Is the simpler model as consistent with all experimental data as the redox model?

The 'scavenger' model

In the alternative model (Figure A1) presented in Appendix B, the free pheromone F interacts directly with the receptor molecules. This model does not employ the redox shift of the PBP as a mechanism of pheromone deactivation. The pheromone is deactivated while bound to B, the only species of the pheromone-binding protein. Thus in the alternative model the PBP acts as a scavenger, not as a carrier ('scavenger model').

The parameters of this model (Figure A2) are the same as in the redox model with two exceptions: $E_{(0)}$ had to be decreased from 400 to 18 nM, in order to match the fall of the receptor potential. As a consequence, the protection of the pheromone bound to PBP had to be weakened by increasing k_{10}, in order to match the velocity of pheromone degradation measured on intact antennae (Figure A4). The increased k_{10} leads to a $K_{m11,12}$ that is lower than in the redox model.

With respect to the responses to 2 s stimuli, the alternative model simulates the receptor potential amplitude, its rise and fall as perfectly as the redox model (Figures A3, A5). There are, however, differences to the redox model, e. g. with respect to the way the model responds to changes of single parameters.

(1) First of all, the alternative model lacks a carrier for the transport of the pheromone towards the receptor cell. In this model, the PBP solubilizes the pheromone by binding but at the same time deactivates it. It does not act as a carrier since the small amount of pheromone dissociating from the complex FB is not sufficient to elicit the receptor potential; it produces the tailing of the receptor potential, after stimulus offset. Increasing the rate constant k_{-7} would merely increase the tailing level beyond the observed values (Figure A7). If also k_7 is increased (to keep K_{d7} the same), the rate of pheromone deactivation due to binding to PBP would be too high. In contrast to this model, the sensillum lymph exchange experiments of Van den Berg and Ziegelberger (Van den Berg and Ziegelberger, 1991) suggest that the pheromone is active while bound to the PBP (see Introduction).

(2) In the alternative model the enzymatic pheromone degradation saturates at lower uptake values than in the redox model. This is due to the lower value of $K_{m10,11}$ in the alternative model (see above). Experimentally, however, a half life of ~3 min has been found over the entire range of stimulus uptake tested, 10^{-1}–10^3 µM/10 s (Kasang, 1971, 1973). Thus the experimental result is better simulated by the redox model (Figure 4), with its higher $K_{m10,11}$.

(3) In contrast to the redox model, the alternative model shows a dependence of the fall of the receptor potential on the enzyme concentration $E_{(0)}$, especially for an increased $E_{(0)}$ (Figure A6). Experimentally, no changes of the kinetics of the receptor potential were detected in antennae that happened to contain <1% of the usual amount of enzyme (Maida et al., 1995). This finding is, however, not suited to distinguish between the two models. The small increase of the fall time expected from the alternative model for a smaller $E_{(0)}$ (Figure A6) was not measurable due to the large variability of the data.

In conclusion, the alternative (scavenger) model is able to simulate the receptor potential kinetics, but is not fully compatible with experimental findings in moth antennae. However, the scavenger model might be valid for olfactory organs where the receptor cells are exposed to the air space, e.g. in vertebrates. It is conceivable that sufficient amounts of odour molecules directly reach parts of the olfactory cilia at the very surface of the mucosa (Reese, 1965; Menco, 1989; Menco and Farbman, 1992) without the help of a carrier protein. The odorant binding proteins in the mucosa could then act as scavengers only.

The 'carrier-to-scavenger' model

In the redox model the PBP has four functions:

1. to solubilize the pheromone and to carry it to the receptor molecule;
2. to protect it, on its way to the receptor, from enzymatic degradation;
3. to mediate the interaction with the receptor; and
4. to keep the pheromone away from the receptors (deactivation, or scavenger function).

As shown below, the described network (Figure 1) applies not only to the redox model, but also to other models in which the PBP switches from a carrier to a scavenger function ('carrier-to-scavenger model'). A number of questions can be addressed in the framework of the redox model.

How does the diffusional transport of the adsorbed pheromone influence the receptor potential?

The diffusion towards the receptor cell of the pheromone molecules adsorbed by the olfactory hairs influences the rise time of the receptor potential. With a diffusion coefficient of $3 \cdot 10^{-7}$ cm^2/s determined for the pheromone migration on the olfactory hairs (Kanaujia and Kaissling, 1985), diffusion is responsible for the initial delay of the receptor potential in the range of 10 ms observed at very strong stimulus intensities. The fall of the receptor potential is not noticeably affected by diffusion. As discussed below, it strongly depends on the pheromone deactivation.

Does the free pheromone or the complex pheromone–PBP interact with the receptor molecule at the receptor cell membrane?

It was shown for the redox model that, due to the large amount of PBP and the rapid association of pheromone and B_{red}, almost no free pheromone exists in the sensillum lymph. Therefore the pheromone interacts with the receptor molecule most likely while bound to the carrier form of the PBP (B_{red}). This gives rise to two further questions: (a) how does the pheromone–PBP binding affect the receptor cell response and (b) why is the PBP concentration so high?

(a) Interestingly, the affinity between the complex FB_{red} and the receptor resulting from the model is much (1000-fold) smaller than that between F and B_{red}, as can be seen by comparing K_{d3} and the measured dissociation constants (Kaissling *et al*. 1985; Du and Prestwich, 1995) (Figure 2). This shows that high sensitivity of the receptor cells, i.e. their response to single pheromone molecules, does not necessarily involve high binding affinity between stimulus and receptor molecules. A similar situation applies for the reception of maltose in *Escherichia coli*. The maltose-binding protein (MBP) occurs in a high concentration (1 mM) in the periplasmic space. Maltose is bound to the MBP with a K_d of 3 μM; the complex of MBP and maltose is bound to the receptor at the cell membrane less strongly, with a K_d of 250 μM (Manson, *et al*., 1985; Bohl *et al*., 1995).

Furthermore, the degree of affinity between pheromone and PBP is not necessarily correlated with the one of the specificity of binding. This is suggested by the observation that the specificity of pheromone–PBP binding was different from and much lower than the specificity of the receptor cell response. Binding and competition assays with PBP and pheromone components as well as their derivatives are reported for *Antheraea* species. In competition experiments with the pheromone component [³H](*E,Z*)-6,11-hexadeca-dienyl acetate and native PBP, 50% reduction of ³H-binding by hexadecanyl acetate, or (*E,Z*)-6,11-hexadecadienol was reached at a 10- or 300-fold higher concentration, respectively (De Kramer and Hemberger, 1987; Prestwich *et al*., 1995; Kaissling, 1998c). Electrophysiological tests showed an ~10 000-fold lower effectiveness of the alcohol and an ~1 000 000-fold lower effectiveness of the saturated acetate

(Kaissling, unpublished). Two recombinant PBPs of *A. pernyi* (Krieger *et al*., 1991) differed by 3- to 16-fold in their affinities for two pheromone components tested (Du and Prestwich, 1995), whereas the effects of the pheromone compounds on the receptor cells differed by ~1000-fold or more (Kaissling, 1987). Examples are seen in Figures 6D and 7B, where the cell tuned to the aldehyde component of the pheromone [(*E,Z*)-6,11-hexadecadienyl] weakly responds to very strong stimulation by the acetate. It should be noted that in *A. polyphemus* three PBPs have been found, that occurred in about the following proportions PBP1 : PBP2 : PBP3 = 100 : <10 : 40 [estimated from Maida *et al*. (Maida *et al*., 2000), where PBP1 = Apol3 of Du and Prestwich (Du and Prestwich, 1995)]. In a recent study, the dissociation constants of (+)- and (–)-disparlure and two recombinant PBPs in the gypsy moth differed by ~2- to 4-fold (Plettner *et al*., 2000). In contrast, the sensitivities of both types of single receptor cells for the two enantiomers differed by factors of >100 (Hansen, 1984). Several authors studied ligand binding in moth PBPs (Feixas *et al*., 1995; Maibeche-Coisne *et al*., 1997; Oldham *et al.*, 2000), honey bees (Danty *et al*., 1999) and beetles (Wojtasek *et al*., 1999). In conclusion, the contribution of pheromone–PBP binding to the specificity of the receptor cells seems to be minor (Steinbrecht, 1996). In addition, according to the redox model, different affinities of the PBP for its ligands would hardly affect the receptor cell response, whereas a significant contribution of the binding to PBP is possible in the scavenger model.

(b) In the redox model, the concentration of PBP does not affect the amplitude or the fall of the receptor potential (Figure 9), except if the PBP concentration is >100-fold reduced. The latter would reduce the proportion Q_1 of pheromone adsorbed that is available to the receptor molecules [equation (A29)] and the sensitivity of the moth important for upwind orientation over long distances (Kaissling and Priesner, 1970; Todd and Baker, 1999). However, already with a 10-fold reduction of the PBP concentration the receptor potential would rise more slowly (Figure 7C). This would impair the temporal resolution of the receptor cells at high stimulus concentrations, where moths respond to each of several odor pulses per second with an upwind turn [reviewed by Kaissling (Kaissling, 1997) and Baker *et al.* (Baker *et al*., 1998)].

How many receptor molecules per membrane area are expected?

The minimum density of receptor molecules in the outer dendrite membrane, determined from equation (13), is in the range of 15% of the value expected for maximum coverage, by 40 000 units/μm^2 of membrane area. The latter value was given by Dratz and Hargrave (Dratz and Hargrave, 1983) for rhodopsin molecules in the disk membrane of visual cells and might apply also for olfactory receptor molecules of insects (Clyne *et al*., 1999; Vosshall

et al., 1999). Maximum coverage of the dendrite area of 426 μm^2 [(Keil, 1984); for identification of the cell type, see Kumar and Keil (Kumar and Keil, 1996)] corresponds to $1.7 \cdot 10^7$ receptor molecules per receptor cell. The above value of $R_{(0)}$ for the receptor cell tuned to the major pheromone component of *A. polyphemus* is preliminary since it is partially based on data from *Bombyx mori*: the rate constants were derived for the bombykal receptor cell (A.V. Minor *et al.*, unpublished data). However, the uncertainty of $R_{(0)}$ is not very large, since the value obtained from equation (13) is a minimum, which is not very far from the maximum estimated from the dendritic membrane area and the above density of rhodopsin.

It should be noted that the (minimum) density of receptor molecules calculated here for *A. polyphemus* (6000/μm^2) is below the one of membrane 'substructures' found in olfactory dendrites of this species—30 000/μm^2 (Klein and Keil, 1984). The density of 'intramembrane particles' counted in olfactory dendrites of the fly *Calliphora vicina* or in cilia of the vertebrate olfactory mucosa was 1200/μm^2 (inner membrane face) and 200/μm^2 (outer face) (Menco and Van der Wolk, 1982; Steinbrecht, 1980). The expected density of ion channels per receptor cell is much smaller, ~25/μm^2 for a conductance per channel of 30 pS (Kaissling and Thorson, 1980; Kaissling and Kumar, 1997; Eschrich *et al.*, 1998).

Could the redox shift of the PBP serve as a deactivation mechanism?

The modeling showed that the redox shift of the PBP observed *in vitro* (Ziegelberger, 1995) could serve as a deactivation mechanism. The velocity of the redox shift measured *in vitro* was 8% of the velocity expected from the modeling analysis of the receptor potential (Kaissling, 1998b); the difference could be due to deteriorating conditions in the homogenate, which might interfere with this process.

Conceivably, the reduced PBP (with one or two disulfide bonds) represents an 'open' form of the protein which binds the pheromone more rapidly than its 'closed' form. It carries the pheromone and possibly 'presents' it to the receptor molecules. The formation of the disulfide bonds by oxidation would turn the PBP into a scavenger that deactivates the pheromone. The redox mechanism is compatible with the finding that saturation of binding was reached with one pheromone molecule per PBP (Kaissling *et al.*, 1985).

In the redox model the dissociation constants used for both forms of the PBP-pheromone complex, K_{d2} and K_{d7}, are the same. However, the respective rate constants for association and dissociation are 1000-fold lower for binding to the scavenger form of the PBP than to its carrier form. This is necessary since k_2 needs to be high to produce enough FB_{red}, whereas k_{-7}, responsible for the tailing of the receptor potential, needs to be minimal.

Is the redox shift catalysed by the receptor molecules or by a separate enzyme?

The fact that the redox shift did not occur with PBP and pheromone alone, but only in the presence of isolated hairs, suggested the existence of a catalysing agent (Ziegelberger, 1995). The previously discussed possibility of receptor molecules acting as catalysts (Kaissling, 1998b) seems less likely in view of recent experiments with decyl-thio-trifluoro-propanone (DTFP) (Pophof, 1998; Pophof *et al.*, 2000), a putative blocker of pheromone receptor molecules. This compound reduced the receptor potential amplitude but did not affect the half time of its fall after stimulus offset. A special reaction network with the receptor molecules as catalysts showed that their blocking would cause a slower fall of the receptor potential. Since this did not occur we now prefer the idea that a postulated enzyme (N) catalyses the redox shift.

In addition to the enzyme N, the redox shift might require an oxidizing cofactor. One candidate cofactor could be the sensory neuron membrane protein 1 (SNMP1) recently discovered in male antennae of *A. polyphemus* and supposed to have a docking function for the stimulus (Rogers *et al.*, 1997). This protein is anchored by two transmembrane domains and has a large extracellular loop containing nine cysteines, at least six of which might be involved in disulfide bonds, as found for the related CD36 protein (Rasmussen *et al.*, 1998).

It should be noted that with physiological stimuli only a minute fraction of B_{red} is converted into B_{ox}, since even with the strongest stimuli the amount of pheromone loaded on the hair is small compared with the abundance of PBP. For this reason a regeneration of B_{ox} to B_{red} has not been included in the network. It is an open question whether the redox shift of the PBP *in vivo* requires the presence of the pheromone. If the shift occurs without the pheromone, the reduced PBP and the oxidizing agent ought to be constantly renewed. Interestingly, a significant turnover of the PBP within a few days has been found in the gypsy moth *Lymantria dispar* (Vogt *et al.*, 1989).

Which alternative mechanisms of pheromone deactivation are to be discussed?

So far the redox shift has been described for one species only, *A. polyphemus*. The redox model, however, can be applied to any mechanism in which the PBP turns from a carrier into a scavenger and in which this process is enzymatically catalysed.

A new mechanism may be proposed here for the case of a binding protein that may exist in the oxidized form only, not showing a redox shift. A possible example is the PBP of *Bombyx mori*, of which the crystal structure has recently been analysed by X-ray diffraction (Sandler *et al.*, 2000). The recombinant protein has three disulfide bonds and shows a hydrophobic binding pocket for the bombykol molecule inside the protein (Sandler *et al.*, 2000). The authors

suggested that the pheromone is released when the complex contacts the plasma membrane of the receptor cell in order to interact with the receptor molecule. In their model the PBP functions as a carrier but not as a scavenger. The release may be caused by conformational changes induced by local charge distributions at the membrane acting like pH changes (Wojtasek and Leal, 1999; Damberger et al., 2000; Sandler et al., 2000). These authors do not discuss how the pheromone enters the inner binding cavity and how it is deactivated.

In contrast, we propose that the pheromone entering the sensillum lymph space is bound to hydrophobic patches on the outer side of the protein, thus being solubilized and transported to the receptor cell. Binding of the pheromone to the outer side could be facilitated by the dimeric structure of the PBP. That the PBP occurs as a dimer was suggested by non-denaturating gel electrophoresis and gel filtration (Kaissling et al., 1985) and finally proven by Campanacci et al. (Campanacci et al., 1999) and Leal (Leal, 2000). Bound to the outer side of the PBP, the pheromone would remain 'visible' to the receptor molecules of the receptor cell membrane. Due to the above pH effects and/or with the help of a catalysing factor, the PBP could become 'open' and 'swallow' the pheromone and thereby deactivate it, i.e. prevent it from interacting further with receptor molecules. This 'carry-and-swallow' mechanism is formally identical with the redox model if FB_{red} and FB_{ox} represent the pheromone bound to an outer and an inner binding site, respectively.

Does the enzymatic pheromone degradation contribute to the kinetics of the receptor potential?

In the redox model, the enzyme E does not contribute significantly to the receptor potential kinetics in a time scale of ~20 s. The importance of enzymatic pheromone degradation can be demonstrated using a pheromone derivative that most likely cannot be degraded by sensillar enzymes. Thus, a brief (1 s) stimulus of the bombykol derivative (Z,E)-4,6-hexadecadiene produced a 'normal' receptor potential of the bombykol receptor cell of *Bombyx mori*. After stimulus offset, however, the receptor cell continued to fire nerve impulses at low rate for ten or more minutes, much longer than after a bombykol stimulus (Kaissling et al., 1989). The markedly prolonged tailing caused by the derivative might indicate that the putative alcohol dehydrogenase metabolizing the alcohol (Kasang et al., 1989b) is not able to degrade the alkene derivative.

In conclusion, the main function of the enzymatic degradation may be to reduce the tailing to zero, i.e. to eliminate the pheromone molecules completely from the hairs and thus maintain the high sensitivity of the receptor cell. This is important since even a small increase of impulse firing above the spontaneous level due to residual pheromone on the hair would seriously impair the threshold sensitivity to a new stimulus.

Is the pheromone protected from enzymatic degradation while bound to the PBP?

The relatively slow pheromone degradation measured on the living antenna (Kasang et al., 1989b) in spite of the fast degradation by the purified enzyme (Vogt et al., 1985) can be explained if the pheromone associated with the antenna is largely protected from enzymatic degradation (Vogt and Riddiford, 1986). However, a partial degradation of the pheromone bound to PBP (especially to B_{ox}) is necessary since otherwise the degradation would take much longer than observed in situ [$t_{1/2}$ = 3 min (Kasang et al., 1988, 1989b)]. Thus an enzymatic degradation of the pheromone in the complex FB_{ox} was introduced in the model, with a 1000-fold smaller association rate of FB_{ox} and E, as compared with the association of F and E. This is an interesting parallel to the 1000-fold lower rate constants of the interaction of pheromone and B_{ox} (reaction 7). Degradations of F to M and FB_{ox} to MB_{ox} have to be considered as separate reaction mechanisms.

Because it promotes the tailing, the protection of the pheromone bound to B_{ox} from enzymatic degradation appears disadvantageous. What is then the advantage of the protection? The biological function of the protection may be to guarantee that the complex FB_{red} remains intact during its transport towards the receptors. The protection of the pheromone bound to B_{red} increases the sensitivity of the system by fivefold. The benefit of the protection of the pheromone on its way towards the receptor cell seems significant if one considers the enormous efforts of male saturniid moths to lower the detection threshold by increasing the size of the antennae. To compensate for a fivefold reduced sensitivity would require a more than fivefold enlarged antenna.

Which reactions are rate-limiting for the receptor potential and responsible for its altered kinetics upon stimulation with pheromone derivatives?

The modeling demonstrates that the kinetics of the cell response may be determined not just by the binding to and activation of the receptor molecule. In both versions of the carrier-to-scavenger model discussed—the redox model and the carry-and-swallow model—the deactivation process significantly contributes to the response characteristics. Especially it affects the transients of the receptor potential, but also its amplitude. In contrast, changes in the receptor activation merely correspond to those obtained by varying the stimulus intensity, with little influence on the transients. Interestingly, the binding affinity to the PBP, both forms, and the enzymatic degradation are of little importance for the responses of the carrier-to-scavenger model, but strongly influence the response kinetics of the alternative 'scavenger' model. The differences between the two models become clear if one considers the initial flows of F to the various reaction partners involved in the pheromone deactivation (Figure 12). The deactivation of F almost
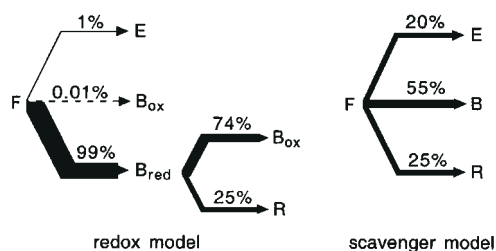
Figure 12   Initial flows of F to various reaction partners in two types of model, calculated from the product of the association rate constant and the concentrations of both binding partners at uptake of 1 µM/s. Total flow = 100%. The deactivation of F works via the switch of the PBP from the carrier form B_{red} to the scavenger form B_{ox} in the redox model, and via E and binding to the scavenger B in the scavenger model. In both models the same fraction of F flows to the receptors R.

exclusively occurs via binding to B_{red} in the redox model, whereas it works via the binding to E and B in the alternative model.

The characteristic variations of the time course of the responses to bombykol homologues observed by Kaissling (Kaissling, 1987, 1998a) could be due to the velocity of the switching from the carrier to the scavenger function. The homologues with shorter chain lengths than bombykol showed a faster time course, possibly indicating a more rapid swallowing. Conceivably, the alcohols enter the binding pocket with the aliphatic end first, and find the docking position at the serine 9 more rapidly if the chain is shorter. Furthermore, the bombykol homologues with even positions of the double bonds (10,12 or 8,10) show a faster time course than those with odd positions (11,13 or 9,11). While entering the binding pocket, those ligands with even positions might more easily adopt the correct hook-like shape of the lipophilic end and, therefore, be swallowed more rapidly. Thus, the change of the PBP from the carrier to the scavenger, catalysed by the enzyme N, may contribute to the high specificity of the receptor cell response. To explain the subtle pattern of the responses to the bombykol homologues by effects on intracellular processes rather than by peripheral interactions seems much more difficult.

In summary, the structure of the ligand could influence rate constants involved in receptor reactions (k_3, k_{-3}, k_4, k_{-4}), but also those involved in the pheromone deactivation (k_5, k_{-5} and k_6). The receptor interaction and the deactivation mechanism can be considered as parallel sets of filters, both of them determining the extraordinary chemical specificity of the receptor cell response. This view applies to any chemoreceptors that are associated with a stimulus deactivation mechanism and seems important to be considered in any structure–activity studies. The binding of the pheromone to the B_{red} in the redox model would correspond to a preceding filter. As shown above, this serial filter plays a minor role for the specificity of the cell response in the carry-to-scavenger model. In the scavenger model binding to E, B and R are

parallel processes all of which may contribute to the response specificity.

How does intracellular signalling contribute to the kinetics of the receptor potential?

The fact that the receptor potential kinetics, including saturation effects and tailing, can be modeled by perireceptor and receptor reactions suggests that these events proceed more slowly than the subsequent intracellular processes leading from receptor activation to the receptor potential. In fact, some intracellular signalling processes observed *in vitro* are extremely fast (Boekhoff *et al.*, 1993; Breer *et al.*, 1994; Stengl *et al.*, 1999). However, a quantitative understanding of these processes *in vivo*, especially for the stimulation by single pheromone molecules is still lacking (Kaissling and Boekhoff, 1993; Kaissling, 1994b, 1996).

Up to this point the model proposed here does not include processes such as adaptation, or desensitization of ion channels, etc. It has been shown that adaptation of pheromone receptor cells occurs, and even local adaptation of a portion of the outer dendrite is possible (Zack, 1979; Kaissling *et al.*, 1987). So far unexplained, and probably depending on intracellular processes, is the shape of the dose–response curve of the receptor potential amplitude at flow equilibrium (Kaissling, 1987). Several physical explanations have been discussed for the slope of this curve, which covers about six decades of stimulus intensity. It could be due in part to electrical cable properties of the sensory dendrite (Kaissling, 1971, 1974; Vermeulen *et al.*, 1997). A further reason, neglected in this analysis, could be distributed affinities of reaction partners of the pheromone involved in reception as well as deactivation (Thorson and Biederman-Thorson, 1974). In this context it would be most interesting to study the alterations of the dose–response curves observed after sensory adaptation (Kaissling, 1972, 1987).

Concluding remarks

In the course of the modeling, gaps in our knowledge became apparent. These had to be bridged by assumptions in order to obtain a functioning model that is compatible with all experimental data obtained so far. One purpose of this approach is to formulate hypotheses in order to stimulate further experiments towards clarification of the functional interrelations of peripheral processes in olfactory reception and to facilitate understanding of their biological significance. Some of the assumptions may be difficult to confirm with the techniques presently available. However, one goal of this paper was to demonstrate that the kinetics of the receptor potential may be governed by perireceptor and receptor events rather than intracellular signalling processes. This idea, first suggested by the observation of saturation effects and ligand-dependent kinetics of the receptor potential (Kaissling, 1972, 1974, 1977, 1998a), is now supported by a quantitative model. Another goal was to demonstrate the multifunctional character of odorant

binding proteins, including their possible switch from the carrier to the scavenger function during olfactory transduction. It should be noted that additional functions have not been discussed. For instance, that the PBP is a significant organic anion is suggested by the excess of negative charges; the PBP may compensate for the lack of anions found by elementary analysis of the sensillum lymph (Kaissling and Thorson, 1980).

Computer modeling

Any set of coupled chemical reactions with associated rate constants, once specified in a chosen syntax, is automatically parsed by our custom computer programs so as to generate a map of the corresponding set of differential equations. Given a set of initial conditions, these are solved by a fifth-order, adaptive Runge–Kutta algorithm [modified from Press *et al*. (Press *et al*., 1992)] for the time courses of the concentrations of all species. The accuracy has been controlled by detailed comparison of complex cases with the Berkeley Madonna Generalized Kinetics Program, the IBM Chemical Kinetics Simulator (CKS) and the standard Electronic Circuit Analysis Programs (ECAP, in DOS). Menu selection within lists of all species involved and parameter-sensitivity analyses elicit autoscaled plots of the transient behaviours of the concentrations of the selected species. This facility is implemented on the Macintosh with C-language control of the Macintoxh User Interface via the code resources provided by MitoSystems Inc. (Santa Monica, CA, USA).

Summary

Olfactory perireceptor and receptor events are considered as a network of chemical reactions between the odorant, an odorant binding protein, hypothetical olfactory receptor molecules, the odorant degrading enzyme E and a postulated enzyme N involved in the rapid deactivation of the odorant. A quantitative model of this network is presented for the pheromone reception of the moth *Antheraea polyphemus*. The model is combined with a model of pheromone diffusion on the cuticular olfactory hair of the moth antenna, using a diffusion coefficient measured for longitudinal diffusion along the hairs. The parameters of the network, including the initial concentration of each reaction partner and the rate constant of each reaction, have been determined experimentally and using assumptions.

Two versions of the network are compared: In the 'carrier-to-scavenger model' the pheromone-binding protein (PBP) first acts as a carrier which binds the pheromone, transports it through the extracellular sensillum lymph, and mediates its interaction with the receptor molecule. Later the PBP turns into a scavenger which deactivates the bound pheromone. The switch from a carrier to a scavenger is catalyzed by a postulated enzyme N. Two possible mechanisms for the switch are discussed, the redox shift found in *vitro* by Ziegelberger (Ziegelberger, 1995) and a 'swallowing' of the pheromone into the binding cavity of the PBP. The latter idea is based on the structure of the bombykol binding protein of *Bombyx mori* analysed recently (Sandler *et al.*, 2000). In the second model, the PBP acts as a scavenger only ('scavenger model'). This model lacks a carrier; the free pheromone interacts with the receptor molecule.

Computer versions of both models simulate the kinetics of the receptor potentials recorded from single olfactory hairs. However, only the carrier-to-scavenger model might apply to the reception of amphiphilic pheromone molecules in insects. The scavenger model could describe events in the vertebrate mucosa where the olfactory cilia might be partially exposed to the air space so that the odorants could contact them directly, without the help of a carrier.

In either model the kinetics of the receptor potential largely reflects the velocity of odorant deactivation, i.e. it depends on the enzyme N in the carrier-to-scavenger model but on the pheromone-degrading enzyme E and the association rate of pheromone and PBP in the scavenger model. In the first model the enzyme E and the binding affinity of pheromone and PBP do not influence the specificity of the receptor cell response, whereas they do so in the second model. Interestingly, the affinity of the binding of the pheromone to the PBP is ~600 fold higher than the affinity between the receptor molecules and the pheromone–PBP complex in the first model, or the free pheromone in the second model.

In both models the pheromone bound to the PBP is partially protected from enzymatic degradation. The protection is important in the first model especially for the pheromone on its way towards the receptor molecule, i.e. while bound to the carrier form of the PBP.

Finally, it has been calculated that the plasma membrane of the receptor cell dendrite is densely covered by receptor molecules, with a minimum value of 15% of full coverage defined by the density of rhodopsin in the discs of visual cells. The number of receptor molecules calculated is >2000-fold smaller than the number of PBP molecules in the olfactory hair.

Acknowledgements

References

Baker, T.C., Fadamiro, H. and **Cossé, A.A.** (1998) *Fine-grained resolution*

of closely spaced odor strands by flying male moths. Nature (Lond.), 393, 530.

Bohl, E., Shuman, H.A. and **Boos, W.** (1995) *Mathematical treatment of the kinetics of binding protein dependent transport systems reveals that both the substrate loaded and unloaded binding proteins interact with the membrane components.* J. Theor. Biol., 172, 83–94.

Boeckh, J. and **Ernst, K.D.** (1987) *Contribution of single unit analysis in insects to an understanding of olfactory function*. J. Comp. Physiol., 161, 549–565.

Boekhoff, I., Seifert, E., Göggerle, S., Lindemann, M., Krüger, B.-W. and **Breer, H.** (1993) *Pheromone-induced second-messenger signaling in insect antennae.* Insect Biochem. Mol. Biol., 23, 757–762.

Breer, H., Raming, K. and **Krieger, J.** (1994) *Signal recognition and transduction in olfactory neurons.* Biochim. Biophys. Acta: Mol. Cell Res., 1224, 277–287.

Campanacci, V., Longhi, S., Nagnan-Le Meillour, P., Cambillau, C. and **Tegoni, M.** (1999) *Recombinant pheromone binding protein 1 from* Mamestra brassicae *(MbraPBP1). Functional and structural characterization.* Eur. J. Biochem., 264,707–716.

Clyne, P.J., Warr, C.G., Freeman, M.R., Lessing, D., Kim, J. and **Carlson, J.R.** (1999) *A novel family of divergent seven transmembrane proteins: candidate odorant receptors in* Drosophila. Neuron, 22, 327–338.

Damberger, F., Nikonova, L., Horst, R., Peng, G.H., Leal, W.S. and **Wuthrich, K.** (2000) *NMR charactertization of a pH-dependent equilibrium between two folded solution conformations of the pheromone-binding protein from* Bombyx mori. Protein Sci., 9, 1038–1041.

Danty, E., Briand, L., Michard-Vanhee, C., Perez, V., Arnold, G., Gaudemer, O., Huet, D., Huet, J.C., Ouali, C., Masson, C. and **Pernollet, J.C.** (1999) *Cloning and expression of a queen pheromone-binding protein in the honeybee: an olfactory-specific, developmentally regulated protein.* J. Neurosci., 19, 7468–7475.

De Kramer, J.J. and **Hemberger, J.** (1987) *The neurobiology of pheromone reception*. In Prestwich, G.D. and Blomquist, G.J. (eds), Pheromone Biochemistry. Academic Press, New York, pp. 433–472.

Del Castillo, J. and **Katz, B**. (1957*) Interaction at end-plate receptors between different choline derivatives*, Proc. R. Soc. Lond. B, 146, 369–381.

Dratz, E.A. and **Hargrave, P.A.** (1983) *The structure of rhodopsin and the rod outer segment disk membrane.* Trends Biochem. Sci., 8, 128.

Du, G.H. and **Prestwich, G.D.** (1995) *Protein structure encodes the ligand binding specificity in pheromone binding proteins.* Biochemistry, 34, 8726–8732.

Eschrich, R., Kumar, G.L., Keil, T.A. and **Guckenberger, R.** (1998) *Atomic force microscopy on the olfactory dendrites of the silkmoths* Antheraea polyphemus *and* A. pernyi. Cell Tiss. Res., 294, 179–185.

Feixas, J., Prestwich, G.D. and **Guerrero, A.** (1995) *Ligand specificity of pheromone binding proteins of the processionary moth*. Eur. J. Biochem., 234, 521–526.

Getchell, T.V., Margolis, F.L. and **Getchell, M.L.** (1984) *Perireceptor and receptor events in vertebrate olfaction*. Progr. Neurobiol., 23, 317–345.

Gnatzy, W., Mohren, W. and **Steinbrecht, R.A.** (1984) *Pheromone receptors in* Bombyx mori *and* Antheraea pernyi. II. *Morphometric analysis.* Cell Tissue Res., 235, 35–42.

Hansen, K. (1984) *Discrimination and production of disparlure enantiomers by the gypsy moth and the nun moth.* Physiological Entomol. 9, 9–18.

Hildebrand, J.G. and **Shepherd, G.M.** (1997) *Mechanisms of olfactory discrimination: Converging evidence for common principles across phyla.* Annu. Rev. Neurosci., 20, 595–631.

Kaissling, K.E. (1971) *Insect olfaction*. In Beidler, L.M. (ed.), Handbook of Sensory Physiology IV. Springer Verlag, Heidelberg, pp. 351–431.

Kaissling, K.E. (1972) *Kinetic studies of transduction in olfactory receptors of* Bombyx mori. In Schneider, D. (ed.), Olfaction and Taste IV. Wissenschaftliche Verlagsgesellschaft, Stuttgart, pp. 207–213.

Kaissling, K.E. (1974) *Sensory transduction in insect olfactory receptors*. In Jaenicke, L. (ed.), Biochemistry of Sensory Functions, 25. Mosbacher Colloquium Gesellschaft Biologische Chemie. Springer, Berlin, pp. 243–273.

Kaissling, K.E. (1977) *Structures of odour molecules and multiple activities of receptor cells.* In Le Magnen, J. and MacLeod, P. (eds), Olfaction and Taste VI. Information Retrieval, London, pp. 9–16.

Kaissling, K.E. (1986) *Chemo-electrical transduction in insect olfactory receptors.* Annu. Rev. Neurosci., 9, 21–45.

Kaissling, K.E. (1987) *R.H. Wright Lectures on Insect Olfaction*. Colbow, K. (ed.), Simon Fraser University, Burnaby, B.C., pp. 1–190.

Kaissling, K.E. (1994a) *Elementary receptor potentials of insect olfactory cells.* In Kurihara, K., Suzuki, N. and Ogawa, H. (eds), Olfaction and Taste XI. Springer, Tokyo, pp. 812–815.

Kaissling, K.E. (1994b) *IP3 effects in moth pheromone receptors: calculations.* In Elsner, N. and Breer, H. (eds), Sensory Transduction, Proceedings of the 22nd Göttingen Neurobiological Conference, Vol I. Thieme, Stuttgart, Abstract 94.

Kaissling, K.E. (1995) *Single unit and electroantennogram recordings in insect olfactory organs.* In Spielman, A.I. and Brand J.G. (eds), Experimental Cell Biology of Taste and Olfaction: Current Techniques and Protocols. CRC Press, Boca Raton, pp. 361–386.

Kaissling, K.E. (1996) *Peripheral mechanisms of pheromone reception in moths.* Chem. Senses, 21, 257–268.

Kaissling, K.E. (1997) *Pheromone-controlled anemotaxis in moths.* In Lehrer, M. (ed.), Orientation and Communication in Arthropods. Birkhaeuser, Basel, pp. 343–374.

Kaissling, K.E. (1998a) *Flux detectors versus concentration detectors: two types of chemoreceptors.* Chem. Senses, 23, 99–111.

Kaissling, K.E. (1998b) *Pheromone deactivation catalyzed by receptor molecules: a quantitative kinetic model.* Chem. Senses, 23, 385–395.

Kaissling, K.E. (1998c) *Olfactory transduction in moths: II. Extracellullar transport, deactivation and degradation of stimulus molecules.* In Taddei-Ferretti, C. and Musio, C. (eds), From Structure to Information in Sensory Systems. World Scientific, Singapore, pp. 113–137.

Kaissling, K.E. and **Boekhoff, I.** (1993) *Transduction and intracellular messengers in pheromone receptor cell of the moth* Antheraea polyphemus. In Wiese, K., Gribakin, F.G., Popov, A.V. and Renninger, G. (eds), Sensory Systems of Arthopods. Birkhäuser, Basel, pp. 489–502.

Kaissling, K.E. and **Kumar, G.L.** (1997) *Densities of putative receptor molecules and ion channels in dendritic membranes of pheromone receptor cells of moths*. In Elsner, N. and Wässle, H. (eds), Proceedings of the 25th Göttingen Neurobiological Conference, Vol. II. Thieme, Stuttgart, p. 429.

Kaissling, K.E. and **Priesner, E.** (1970) *Die Riechschwelle des Seidenspinners.* Naturwissenschaften, 57, 23–28.

Kaissling, K.E. and **Thorson, J.** (1980) *Insect olfactory sensilla: structural, chemical and electrical aspects of the functional organisation.* In Sattelle, D.B., Hall, L.M. and Hildebrand, J.G. (eds), Receptors for

Neurotransmitters, Hormones and Pheromones in Insects. Elsevier/North-Holland Biomedical Press, Amsterdam, pp. 261–282.

Kaissling, K.E., Klein, U., de Kramer, J.J., Keil, T.A., Kanaujia, S. and **Hemberger J.** (1985) *Insect olfactory cells: electrophysiological and biochemical studies.* In Changeux, J.P. and Hucho, F. (eds), Molecular Basis of Nerve Activity. Proceedings of the International Symposium in Memory of D. Nachmansohn. Walter de Gruyter, Berlin, pp. 173–183.

Kaissling, K.E., Zack Strausfeld, C. and **Rumbo, E.R.** (1987) *Adaptation processes in insect olfactory receptors. Mechanisms and behavioral significance.* Olfaction and Taste IX. Ann. NY Acad. Sci., 510, 104–112.

Kaissling, K.E., Meng, L.Z. and **Bestmann, H.J.** (1989) *Responses of Bombykol receptor cells to (Z,E)-4,6-hexadecadiene and linalool.* J. Comp. Physiol. A, 165, 147–154.

Kanaujia, S. and **Kaissling, K.E.** (1985) *Interactions of pheromone with moth antennae: adsorption, desorption and transport.* J. Insect Physiol., 31, 71–81.

Kasang, G. (1971) *Bombykol reception and metabolism on the antennae of the silkmoth* Bombyx mori. In Ohloff, G. and Thomas, A.F. (eds), Gustation and Olfaction. Academic Press, London, pp. 245–250.

Kasang, G. (1973) *Physikochemische Vorgänge beim Riechen des Seidenspinners.* Naturwissenschaften, 60, 95–101.

Kasang, G. and **Kaissling, K. E.** (1972) *Specificity of primary and secondary olfactory processes in* Bombyx *antennae.* In Schneider, D. (ed.), Olfaction and Taste VI. Wissenschaftliche Verlagsgesellschaft, Stuttgart, pp. 200–206.

Kasang, G., von Proff, L. and **Nicholls, M.** (1988) *Enzymatic conversion and degradation of sex pheromones in antennae of the male silkworm moth* Antheraea polyphemus. Z. Naturforsch., 43c, 275–284.

Kasang, G., Nicholls, M., Keil, T.A. and **Kanaujia, S.** (1989a) *Enzymatic conversion of sex pheromones in olfactory hairs of the male silkworm moth* Antheraea polyphemus. Z. Naturforsch., 44c, 920–926.

Kasang, G., Nicholls, M. and **von Proff, L.** (1989b) *Sex pheromone conversion and degradation in antennae of the male silkworm moth* Bombyx mori L. Experientia, 45, 81–87.

Keil, T.A. (1984) *Reconstruction and morphometry of silkmoth olfactory hairs: a comparative study of sensilla trichodea on the antennae of male* Antheraea polyphemus *and* Antheraea pernyi *(Insecta, Lepidoptera).* Zoomorphology, 104, 147–156.

Keil, T.A. and **Steinbrecht, R.A.** (1984) *Mechanosensitive and olfactory sensilla of insects.* In King, R.C. and Akai, H. (eds), Insect Ulstructure, Vol. 2. Plenum Press, New York, pp. 477–516.

Klein, U. (1987) *Sensillum-lymph proteins from antennal olfactory hairs of the moth* Antheraea polyphemus *(Saturniidae).* J. Insect Biochem., 17, 1193–1204.

Klein, U. and **Keil, T.A.** (1984) *Dendritic membrane from insect olfactory hairs: isolation method and electron microscopic observations.* Cell. Mol. Neurobiol., 4, 385–396.

Krieger, J., Raming, K. and **Breer, H.** (1991) *Cloning of genomic and complementary DNA encoding insect pheromone binding proteins: evidence for microdiversity.* Biochim. Biophys. Acta, 1088, 277–284.

Kumar, G.L. and **Keil, T.A.** (1996) *Pheromone stimulation induces cytoskeletal changes in olfactory dendrites of male silkmoths (Lepidoptera, Saturniidae, Bombycidae).* Naturwissenschaften, 83, 476–478.

Lauffenburger, D.A. and **Linderman, J.J.** (1993) Receptors: Models for Binding, Trafficking and Signaling. Oxford University Press, New York, p. 365.

Leal, W.S. (2000) *Duality monomer–dimer of the phermone-binding protein from* Bombyx mori. Biochem. Biophys. Res. Commun., 268, 521–529.

Maibeche-Coisne, M., Sobrio, F., Delaunay, T., Lettere, M., Dubroca, J., Jacquin-Joly, E. and **Nagnan-LeMeillour, P.** (1997) *Pheromone binding proteins in the moth* Mamestra brassicae*: specificity of ligand binding.* Insect Biochem. Mol. Biol., 27, 213–221.

Maida, R., Ziegelberger, G. and **Kaissling, K.E.** (1995) *Esterase activity in the olfactory sensilla of the silkmoth* Antheraea polyphemus. NeuroReport, 6, 822–824.

Maida, R., Krieger, J., Gebauer, Th., Lange, U. and **Ziegelberger, G.** (2000) *Three pheromone-binding proteins in olfactory sensilla of the two silkmoth species* Antheraea polyphemus *and* Antheraea pernyi. Eur. J. Biochem., 267, 2899–2908.

Manson, M.D., Boos, W., Bassford, P.J., Jr and **Rasmussen, B.A.** (1985) *Dependence of maltose transport and chemotaxis on the amount of maltose-binding protein.* J. Biol. Chem., 260, 9727–9733.

Menco, B.P.M. (1989) *Olfactory and nasal respiratory epithelia, and foliate taste buds visualized with rapid-freeze freeze substitution and lowicryl K11M embedding. Ultrastructural and initial cytochemical studies.* Scan. Microsc., 3, 257–272.

Menco, B.P.M. and **Farbman, A.** (1992) *Ultrastructural evidence for multiple mucous domains in frog olfactory epithelium.* Cell Tissue Res., 270, 47–56.

Menco, B.P.M. and **Van der Wolk, F.M.** (1982) *Freeze-fracture characteristics of insect gustatory and olfactory sensilla. I. A comparison with vertebrate olfactory receptor cells with special reference to ciliary components.* Cell Tissue Res., 223, 1–27.

Meng, L.Z., Wu, C.H., Wicklein, M., Kaissling, K.E. and **Bestmann, H.J.** (1989) *Number and sensitivity of three types of pheromone receptor cells in* Antheraea pernyi *and* A. polyphemus. J. Comp. Physiol. A, 165, 139–146.

Oldham, N.J., Krieger, J. Breer, H., Fischedick, A., Hoskovec, M. and **Svatos, A.** (2000) *Analysis of the silkworm moth (pheromone binding protein-pheromone) complex by electrospray ionization-mass spectrometry.* Angew. Chemie, 112, 4521–4523.

Pelosi, P. (1996) *Perireceptor events in olfaction.* J. Neurobiol., 30, 3–19.

Plettner, E., Lazar, J., Prestwich, E.G. and **Prestwich, G.D.** (2000) *Discrimination of pheromone enantiomers by two pheromone binding proteins from the gypsy moth* Lymantria dispar. Biochemistry 39, 8953–8962.

Pophof, B. (1998) *Inhibitors of sensillar esterase reversibly block the responses of moth pheromone receptor cells.* J. Comp. Physiol. A, 183, 153–164.

Pophof, B., Gebauer, T. and **Ziegelberger, G.** (2000) *Decyl-thiotrifluoropropanone, a competitive inhibitor of moth pheromone receptors.* J. Comp. Physiol. A, 186, 315–323.

Press, W.H., Teukolksky, S.A., Vetterling, W.T. and **Flannery, B.P.** (1992) *Numerical Recipes in C*, 2nd edn. Cambridge University Press, Cambridge.

Prestwich, G.D., Du, G. and **LaForest, S.** (1995) *How is pheromone specificity encoded in proteins?* Chem. Senses, 20, 461–469.

Prestwich, G.D. (1996) *Proteins that smell: pheromone recognition and signal transduction.* Bioorg. Med. Chem., 4, 505–513.

Raming, K. Krieger, J. and **Breer, H.** (1989) *Molecular cloning of an insect pheromone-binding protein.* FEBS Lett., 356, 215–218.

Rasmussen, J.T., Berglund, L., Rasmussen, M.S. and Petersen, T.E. (1998) *Assignment of disulfide bridges in bovine CD36*. Eur. J. Biochem., 257, 488–494.

Reese, T.S. (1965) *Olfactory cilia in the frog*. J. Cell Biol., 25, 209–230.

Rogers, M.E., Sun, M., Lerner, M.R. and Vogt, G. (1997) *SNMP-1, a novel membrane protein of olfactory neurons of the silk moth* Antheraea polyphemus *with homology to the CD36 family of membrane proteins*. J. Biol. Chem., 272, 14792–14799.

Rospars, J.P., Krivan, V. and Lánský, P. (2000) *Perireceptor and receptor events in olfaction. Comparison of concentration and flux detectors: a modeling study*. Chem. Senses, 25, 293–311.

Sandler, B.H., Nikonova, L., Leal, W.S. and Clardy, J. (2000) *Sexual attraction in the silkworm moth: structure of the pheromone-binding-protein–bombykol complex.* Chem. Biol., 7, 143–151.

Schneider, D. (1992) *100 years of pheromone research, an essay on Lepidoptera*. Naturwissenschaften, 79, 241–250.

Steinbrecht, R.A. (1973) *Der Feinbau olfaktorischer Sensillen des Seidenspinners (Insecta, Lepidoptera)*. Z. Zellforsch., 139, 533–565.

Steinbrecht, R.A. (1980) *Cryofixation without cyroprotectants. Freeze substitution and freeze etching of an insect olfactory receptor*. Tissue Cell, 12, 73–100.

Steinbrecht, R.A. (1996) *Are odorant-binding proteins involved in odorant discrimination?* Chem. Senses, 21, 719–727.

Steinbrecht, R.A. (1997) *Pore structures in insect olfactory sensilla: a review of data and concepts*. Int. J. Insect Morphol. Embryol., 26, 229–245.

Steinbrecht, R.A. and Müller, B. (1971*) On the stimulus conducting structures in insect olfactory receptors*. Z. Zellforsch., 117, 570–575.

Stengl, M., Ziegelberger, G., Boekhoff, I. and Krieger, J. (1999) *Perireceptor events and transduction mechanisms in insect olfaction*. In Hansson, B.S. (ed.), Insect Olfaction. Springer, Berlin, pp. 49–66.

Thorson, J. and Biederman-Thorson, M. (1974) *Distributed relaxation processes in sensory adaptation*. Science, 183, 161–172.

Todd, J.L. and Baker, T.C. (1999) *Function of peripheral olfactory organs*. In Hansson, B.S. (ed.), Insect Olfaction. Springer, Berlin, pp. 67–96.

Van den Berg, M.J. and Ziegelberger, G. (1991) *On the function of the pheromone binding protein in the olfactory hairs of* Antheraea polyphemus. J. Insect Physiol., 37, 79–85.

Vermeulen, A., Lánský, P., Tuckwell, H. and Rospars, J.-P. (1997) *Coding of odour intensity in a sensory neuron*. BioSystems, 40, 203–210.

Vogt, R.G. (1987) *The molecular basis of pheromone reception: its influence on behavior*. In Prestwich, G.D. and Blomquist, G.J. (eds), Pheromone Biochemistry. Academic Press, New York, pp. 385–431.

Vogt, R.G. and Riddiford, L.M. (1981) *Pheromone binding and inactivation by moth antennae*. Nature (Lond.), 293, 161–163.

Vogt, R.G. and Riddiford, L.M., (1986) *Pheromone reception: a kinetic equilibrium*. In Payne, T.L., Birch, M.C. and Kennedy, C.E.J. (eds), Mechanisms in Insect Olfaction. Clarendon Press, Oxford, pp. 201–208.

Vogt, R.G., Riddiford, L.M. and Prestwich, G.D. (1985) *Kinetic properties of a pheromone degrading enzyme: the sensillar esterase of* Antheraea polyphemus. Proc. Natl Acad. Sci. USA, 82, 8827–8831.

Vogt, R.G., Köhne, A.C., Dubnau, J.T. and Prestwich, G.D. (1989). *Expression of pheromone binding proteins during antennal development in the Gypsy moth* Lymantria dispar. J. Neurosci., 9, 3332–3346.

Vogt, R.G., Callahan, F.E., Rogers, M.E. and Dickens, J.C. (1999) *Odorant binding protein diversity and distribution among the insect orders, as indicated by LAP, an OBP-related protein of the true bug* Lygus lineolaris (*Hemiptera, Heteroptera*). Chem. Senses, 24, 481–495.

Vosshall, L.B., Amrein, H., Morozov, P.S., Rzhetsky, A. and Axel, R. (1999) *A spatial map of olfactory receptors expression in the* Drosophila antennae. Cell, 96, 725–736.

Wojtasek, H. and Leal, S.W. (1999) *Conformational change in the pheromone-binding protein from* Bombyx mori *induced by pH and by interaction with membranes*. J. Biol. Chem., 274, 30950–30956.

Wojtasek, H., Picimbon, J.-F. and Leal, S.W. (1999) *Identification and cloning of odorant binding proteins from the scarab beetle* Phylloperta diversa. Biochem. Biophys. Res. Commun., 263, 832–837.

Zack, C. (1979) *Sensory adaptation in the sex pheromone receptor cells of saturniid moths.* Diss. Fak. Biol. LMU München, 1–99.

Ziegelberger, G. (1995) *Redox-shift of the pheromone-binding protein in the silkmoth* Antheraea polyphemus. Eur. J. Biochem., 232, 706–711.

Appendix A

The following equations are used to discuss the model

$$\frac{dF}{dt} = U - k_2 \cdot F \cdot B_{red} + k_{-2} \cdot FB_{red} - k_7 \cdot F \cdot B_{ox} + k_{-7} \cdot FB_{ox} - k_8 \cdot F \cdot E + k_{-8} \cdot FE \tag{A1}$$

$$\frac{dFE}{dt} = +k_8 \cdot F \cdot E - k_{-8} \cdot FE - k_9 \cdot FE \tag{A2}$$

$$\frac{dM}{dt} = +k_9 \cdot FE \approx +\frac{k_9 \cdot E_{(0)} \cdot F}{K_{m8,9}} \left(\text{for } F \ll K_{m8,9} \right) \tag{A3}$$

$$\frac{dFB_{red}}{dt} = +k_2 \cdot F \cdot B_{red} - k_{-2} \cdot FB_{red} - k_3 \cdot FB_{red} \cdot R + k_{-3} \cdot FB_{red}R - k_5 \cdot FB_{red} \cdot N + k_{-5} \cdot FB_{red}N - k_{12} \cdot FB_{red} \cdot E + k_{-12} \cdot FB_{red}E \tag{A4}$$

$$\frac{dFB_{red}R}{dt} = +k_3 \cdot FB_{red} \cdot R - k_{-3} \cdot FB_{red}R - k_4 \cdot FB_{red}R + k_{-4} \cdot FB_{red}R' \tag{A5}$$

$$\frac{dFB_{red}R'}{dt} = +k_4 \cdot FB_{red}R - k_{-4} \cdot FB_{red}R' \tag{A6}$$

$$\frac{dFB_{red}N}{dt} = +k_5 \cdot B_{red} \cdot N - k_{-5} \cdot FB_{red}N - k_6 \cdot FB_{red}N \tag{A7}$$

$$\frac{dFB_{ox}}{dt} = +k_6 \cdot FB_{red}N + k_7 \cdot F \cdot B_{ox} - k_{-7} \cdot FB_{ox} - k_{10} \cdot FB_{ox} \cdot E + k_{-10} \cdot FB_{ox}E \tag{A8}$$

$$\frac{dFB_{ox}E}{dt} = +k_{10} \cdot FB_{ox} \cdot E - k_{-10} \cdot FB_{ox}E - k_{11} \cdot FB_{ox}E \tag{A9}$$

$$\frac{dFB_{red}E}{dt} = +k_{12} \cdot FB_{red} \cdot E - k_{-12} \cdot FB_{red}E - k_{13} \cdot FB_{red}E \tag{A10}$$

$$\frac{dMB_{ox}}{dt} = +k_{11} \cdot FB_{ox}E \tag{A11a}$$

$$\frac{dMB_{red}}{dt} = +k_{13} \cdot FB_{red}E \tag{A11b}$$

Equations (A1), (A4) and (A8) can be simplified if certain mass flows in relation to other flows are very small. In equation (A1) we have $k_{-2} \cdot FB_{red} << k_2 \cdot F \cdot B_{red}$, and also both flows of reaction 7 are $<<k_2 \cdot F \cdot B_{red}$. Thus equation (A1) becomes

$$\frac{dF}{dt} \approx U - k_2 \cdot F \cdot B_{red} - k_8 \cdot F \cdot E + k_{-8} \cdot FE \tag{A12}$$

If the flows of reaction 12 are much smaller than those of reaction 5 and if $k_{-2} \cdot FB_{red} << k_2 \cdot F \cdot B_{red}$, equation (A4) becomes

$$\frac{dFB_{red}}{dt} \approx +k_2 \cdot F \cdot B_{red} - k_3 \cdot FB_{red} \cdot R + k_{-3} \cdot FB_{red}R - \\ k_5 \cdot FB_{red} \cdot N + k_{-5} \cdot FB_{red}N \tag{A13}$$

If the flows of reactions 7 and 10 are very small, equation (A8) becomes

$$\frac{dFB_{ox}}{dt} \approx +k_6 \cdot FB_{red}N = +\frac{k_6 \cdot N_{(0)} \cdot FB_{red}}{K_{m5,6}} \tag{A14}$$

At constant uptake U flow equilibrium is reached. From equations (A2) and (A12) set to zero and from (A3) for $F < K_{m8,9}$ we obtain

$$U \approx k_2 \cdot F \cdot B_{red} + k_9 \cdot FE \approx k_2 \cdot F \cdot B_{red} + \frac{k_9 \cdot E_{(0)} \cdot F}{K_{m8,9}} \tag{A15}$$

In the following all equilibrium constants are defined for mono- and bimolecular reactions. The equations (A16), (A20), (A22) and (A23) do not apply for the situation in the network.

$$K_{d2} = \frac{k_{-2}}{k_2} = \frac{F \cdot B_{red}}{FB_{red}} \tag{A16}$$

$$K_{d3} = \frac{k_{-3}}{k_3} = \frac{FB_{red} \cdot R}{FB_{red}R} \tag{A17}$$

$$K_4 = \frac{k_{-4}}{k_4} = \frac{FB_{red}R}{FB_{red}R'} = \frac{FB_{red}R_{max}}{FB_{red}R'_{max}} \tag{A18}$$

$$K_{m5,6} = \frac{k_{-5} + k_6}{k_5} = \frac{FB_{red} \cdot N}{FB_{red}N} \tag{A19}$$

$$K_{d7} = \frac{k_{-7}}{k_7} = \frac{F \cdot B_{ox}}{FB_{ox}} \tag{A20}$$

$$K_{m8,9} = \frac{k_{-8} + k_9}{k_8} = \frac{F \cdot E}{FE} \tag{A21}$$

$$K_{m10,11} = \frac{k_{-10} + k_{11}}{k_{10}} = \frac{FB_{ox} \cdot E}{FB_{ox}E} \tag{A22}$$

$$K_{m12,13} = \frac{k_{-12} + k_{13}}{k_{12}} = \frac{FB_{red} \cdot E}{FB_{red}E} \tag{A23}$$

Furthermore, we set

$$E_{(0)} = E + FE + FB_{red}E + FB_{ox}E \tag{A24}$$

$$E_{(0)} \approx E + FE \quad (\text{for } FB_{red}E + FB_{ox}E << E + FE) \tag{A25}$$

$$R_{(0)} = R + FB_{red}R + FB_{red}R' = R + \frac{FB_{red}R}{Q_4} \tag{A26}$$

(from equations A18 and A32)

$$R_{(0)} \approx FB_{red}R_{max} + FB_{red}R'_{max} = R + \frac{FB_{red}R_{max}}{Q_4} \tag{A27}$$

$$N_{(0)} = N + FB_{red}N \tag{A28}$$

$$Q_1 = \frac{k_2 \cdot F \cdot B_{red}}{U} = 0.99 \approx \frac{1}{1 + \dfrac{k_9 \cdot E_{(0)}}{K_{m8,9} \cdot k_2 \cdot B_{red}}} \tag{A29}$$

(from equation A15)

$$Q_2 = \frac{k_6 \cdot N_{(0)}}{K_{m5,6}} = 0.924 \, / \, s \tag{A30}$$

$$Q_3 = \frac{r_{ERP}}{U} = 0.25 \tag{A31}$$

$$Q_4 = \frac{k_{-4}}{k_4 + k_{-4}} = \frac{1}{\dfrac{1}{K_4} + 1} = \frac{FB_{red}R_{max}}{R_{(0)}} = 0.852 \tag{A32}$$

$$Q_5 = \frac{k_4}{k_4 + k_{-3}} = 0.680 \tag{A33}$$

The dose–response relationship for $FB_{red}R'$ at flow equilibrium is derived as follows. For the flow equilibrium we get from equations (A7), (A13) and (A29)

$$k_6 \cdot FB_{red}N \approx U \cdot Q_1 \tag{A34}$$

Using this equation and equations (A19) and (A17) we obtain

$$\frac{FB_{red}R}{R} \approx \frac{U \cdot Q_1 \cdot K_{m5,6}}{K_{d3} \cdot k_6 \cdot N} \tag{A35}$$

With equations (A26), (A28), (A34) and (A35) we find

$$\frac{FB_{red}R}{R_{(0)}} \approx \frac{1}{\dfrac{K_{d3}}{K_{m5,6}}\left(\dfrac{k_6 \cdot N_{(0)}}{U \cdot Q_1} - 1\right) + \dfrac{1}{Q_4}} \tag{A36}$$

Due to equations (A18) and (A27)

$$\frac{FB_{red}R}{R_{(0)}} \approx \frac{FB_{red}R' \cdot Q_4}{FB_{red}R'_{max}} \qquad (A37)$$

Combining equations (A36) and (A37) we arrive at

$$\frac{FB_{red}R'}{FB_{red}R'_{max}} \approx \frac{1}{\dfrac{K_{d3} \cdot Q_4}{K_{m5,6}}\left(\dfrac{k_6 \cdot N_{(0)}}{U \cdot Q_1} - 1\right) + 1} \qquad (A38)$$

For

$$\frac{K_{d3} \cdot Q_4}{K_{m5,6}} = 1 \qquad (A39)$$

(assumption F) we find

$$\frac{FB_{red}R'}{FB_{red}R'_{max}} \approx \frac{U \cdot Q_1}{k_6 \cdot N_{(0)}} \qquad (A40)$$

which shows a linear dependence of $FB_{red}R'$ on U. If we set this expression $= 1$ we find

$$k_6 \cdot N_{(0)} \approx U_{sat} \cdot Q_1 \qquad (A41)$$

For determining $R_{(0)}$ we use equations (A31) and (A33) and a small uptake with $R \approx R_{(0)}$

$$r_{ERP} = \frac{k_3 \cdot R_{(0)} \cdot FB_{red} \cdot k_4}{(k_4 + k_{-3})} \equiv k_3 \cdot R_{(0)} \cdot FB_{red} \cdot Q_5 = Q_3 \cdot U \qquad (A42)$$

From (A19), (A34) and (A30) we obtain for small uptake where $N \approx N_{(0)}$

$$\frac{k_6 \cdot N_{(0)} \cdot FB_{red}}{K_{m5,6}} \equiv Q_2 \cdot FB_{red} \approx Q_1 \cdot U \qquad (A43)$$

Equations (A41)–(A43) and (A17) reveal

$$R_{(0)} \approx \frac{Q_2 \cdot Q_3}{k_3 \cdot Q_1 \cdot Q_5} = \frac{Q_3 \cdot K_{d3} \cdot U_{sat}}{K_{m5,6}} \cdot \frac{(k_{-3} + k_4)}{k_{-3} \cdot k_4} \qquad (A44)$$

After introducing Q_4 [see equation (A32)]

$$R_{(0)} \approx \frac{Q_3 \cdot K_{d3} \cdot Q_4 \cdot U_{sat}}{K_{m5,6}} \cdot \frac{(k_{-3} + k_4) \cdot (k_{-4} + k_4)}{k_{-3} \cdot k_4 \cdot k_{-4}} \qquad (A45)$$

we find

$$R_{(0)} \approx \frac{Q_3 \cdot K_{d3} \cdot Q_4 \cdot U_{sat}}{K_{m5,6}} \cdot \left(\frac{1}{k_{-3}} + \frac{1}{k_4} + \frac{1}{k_{-4}} + \frac{k_4}{k_{-3} \cdot k_{-4}}\right) \qquad (A46)$$

For

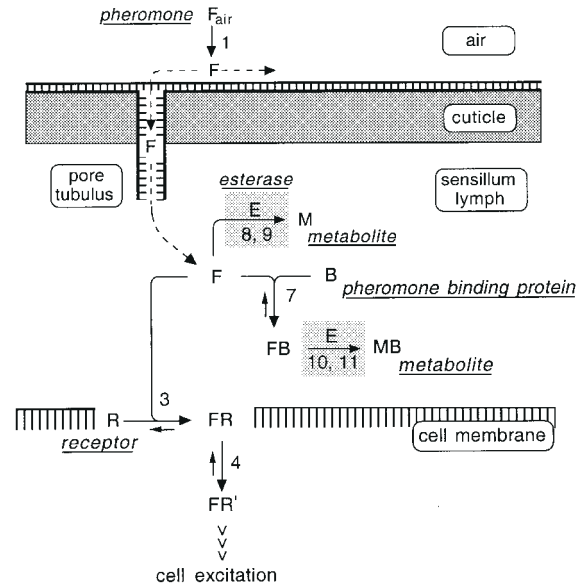$$\frac{K_{d3} \cdot Q_4}{K_{m5,6}} = 1$$

Figure A1 Alternative model: simplified, hypothetical reaction network of perireception and receptor events. The reactions 2, 5, 6, 12 and 13 were omitted. Numbering of the remaining reactions is the same as in the redox model (cf. Figure 1). **(1)** Adsorption of the pheromone F on the surface of the olfactory hair and diffusion towards the receptor cell. **(3)** Binding of F to the receptor molecule R at the receptor cell membrane. **(4)** Activation of the complex FR. **(7)** Binding of F and B (pheromone deactivation). **(8, 9)** Enzymatic degradation of F into the metabolite M by the enzyme E (sensillar esterase). **(10, 11)** Degradation of the complex FB by E into MB. Small arrows indicate reverse reactions. Reactions 9 and 11 are assumed to be irreversible.

(assumption F) we find

$$R_{(0)} \approx Q_3 \cdot U_{sat} \cdot \left(\frac{1}{k_{-3}} + \frac{1}{k_4} + \frac{1}{k_{-4}} + \frac{k_4}{k_{-3} \cdot k_{-4}}\right) \qquad (A47)$$

Appendix B

Alternative model without redox shift

In the alternative model (Figure A1) the pheromone encounters three reaction partners, the receptor molecules R (reaction 3), the pheromone-binding protein, which occurs as only one species B (reaction 7), and the enzyme E (reactions 8 and 9). The assumptions B and D of the redox model are changed. Only the free pheromone F activates the receptor molecules (alternative assumption B). The pheromone is deactivated while bound to B (alternative assumption D).

Since the complex FB does not interact with the receptor molecule, the PBP acts as a scavenger but not as a carrier. The model lacks a carrier; it is called the scavenger model. In this model, B corresponds to B_{ox} of the redox model (also called the carrier-to-scavenger model). Compared with the latter model, reactions 2, 5, 6, 11 and 13 are omitted; the numbering of the remaining reactions is kept the same as in the redox model (Figure A2). Also the initial concentrations and the rate constants are retained, with the exception of $E_{(0)}$; it had to be decreased to 4.5% of the value for the redox model in order to fit the fall of the model receptor potential (Figure A3B). Furthermore, due to the reduced

	k_i (forward)	k_{-i} (reverse)	
k_3	0.209/(s · µM)	7.9/s*	K_{d3} = 37.7 µM
k_4	16.8/s*	98/s*	K_4 = 5.8
k_7	0.000,17/(s · µM)	0.000,01/s	K_{d7} = 60 nM
k_8	150/(s · µM)	300/s	} $K_{m8,9}$ = 2.2 µM
k_9	30	–·–	
k_{10}	3.3/(s · µM)	300/s	} $K_{m10,11}$ = 100 µM
k_{11}	30/s	–·–	

$$R_{(0)} = 1.64 \text{ µM} \qquad B_{(0)} = 4 \text{ mM} \qquad E_{(0)} = 18 \text{ nM}$$

Figure A2 Parameters of the alternative model (Figure A1). The parameters are the same as for the redox model (Figure 2), except that $E_{(0)}$ = 18 nM and k_{10} = 3.33/(µM · s). Asterisks denote values obtained from *Bombyx mori*.
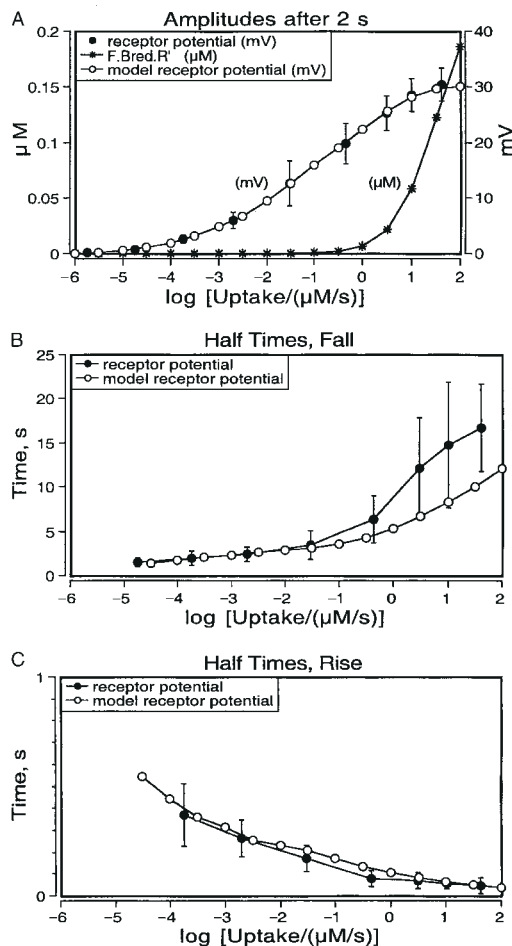

Figure A3 Dose–response functions of the receptor potential recorded (dots); comparison with the alternative model (circles) (cf. Figure 3). Abscissa: stimulus uptake U. Circles: responses of the alternative model using the parameters given in Figure A2. **(A)** Steady amplitudes reached after stimulation for 2 s. **(B, C)** Half times of the transients of the receptor potentials.
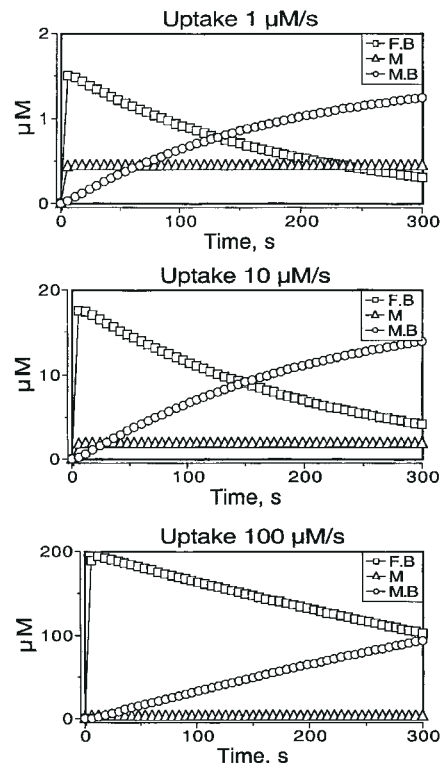

Figure A4 Alternative model, pheromone degradation at different uptake values; stimulus duration 2 s. At an uptake of 100 µM/s the enzyme E is near to saturation which increases the half life of the pheromone (mostly bound to B).

concentration of the degrading enzyme E, the protection of the pheromone bound to B from enzymatic degradation had to be weakened by increasing k_{10} by the reciprocal factor 22, in order to obtain the same half life of pheromone as in the redox model (~2 min). This implies an affinity of E and FB that is 22-fold higher than in the redox model. A consequence of the higher affinity is an earlier saturation of the pheromone degradation indicated by a longer half life of the pheromone (Figure A4, at uptake 100 µM/s).

With these modifications the fall and rise times of the receptor potential could be fitted in the same way as with the redox model (Figure A3B and C). For a stimulus uptake of 1 µM/s the alternative model shows a time course of F very different from that of F in the redox model, but similar to that of FB_{red}; the time courses of FB and MB correspond approximately to those of FB_{ox} and MB_{ox} in the redox model, respectively (compare Figures A5 and 5).

Varying the parameters $R_{(0)}$, k_3, k_{-3}, k_4 and k_{-4} of the alternative model produced effects similar to those found with the redox model (compare Figures A6 and 8). In contrast to the redox model, the variation of $E_{(0)}$ and of the rate constants k_8, k_{-8} and k_9 affects the amplitude and fall of the receptor potential. The fall is much more rapid with more enzyme (Figure A6), larger k_8, and k_9, and with a smaller k_{-8} (not shown). Decreasing the concentration of $E_{(0)}$ has almost no effect. Strong effects on the fall are observed also upon changes of $B_{(0)}$ and k_7, but not with k_{-7} (Figure A7). Increasing k_{-7} increases the level of tailing as in the redox model (cf. Figures A7 and 9).
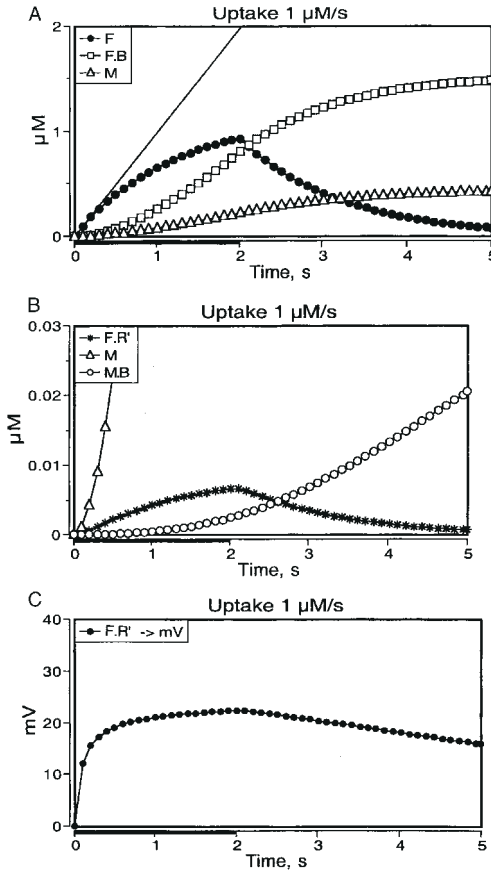
Figure A5   Time course of model variables after a 2 s stimulus (cf. Figure 5). Model parameters as in Figure A2. The concentration of the free pheromone F (**panel A**) shows a time course similar to that of FB_{red} in the redox model (Figure 5A). The concentration of MB parallels that of MB_{ox} (Figure 5B).
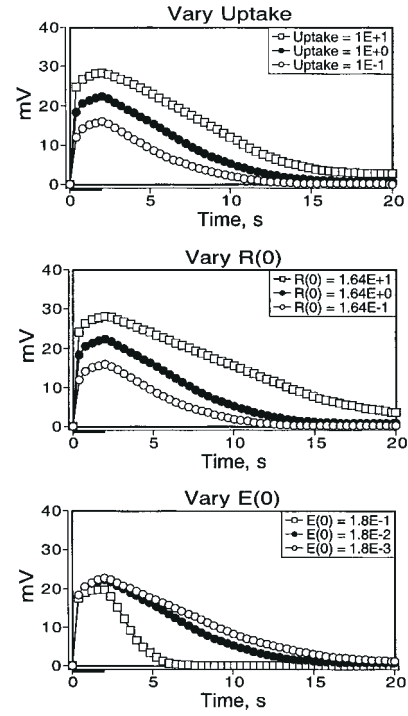

Figure A6   Receptor potentials generated by the alternative model upon variation by factors of ten of the pheromone uptake, of the receptor concentration $R_{(0)}$, and of the enzyme concentration E. The standard pheromone uptake was 1 μM/s (dots), the stimulus duration 2 s. In contrast to the redox model (Figure 11E), the concentration of E and also the rate constants of reactions 8 and 9 (not shown) control the fall of the receptor potential.
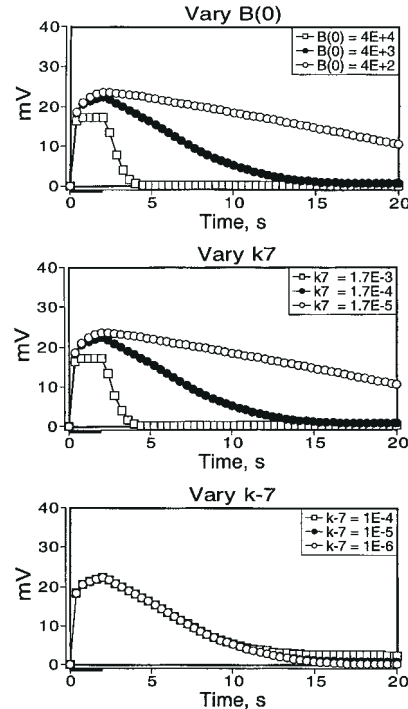
The effects on the kinetics of the receptor potential of variations of $E_{(0)}$ and $B_{(0)}$ are due to the much higher concentration of F in the scavenger model as compared with the redox model (see above). With an uptake of 1 μM/s we find the following concentrations at the end of a 2 s stimulus

$$F = 0.93\ \mu M \qquad FB = 0.80\ \mu M \qquad M = 0.22\ \mu M$$

At 8 s after stimulation offset we have

$$F = 0.001\ \mu M \qquad FB = 1.50\ \mu M \qquad M = 0.44\ \mu M$$

During stimulation, there is much more of F available for the enzymatic degradation than in the redox model. For the scavenger model at low values of the uptake, the direct production of M (dM/dt) via E and the initial flow of F to B can be obtained from the following equations:

$$\frac{dM}{dt} = \frac{k_9 \cdot E_{(0)} \cdot F}{K_{m8,9}} = 0.245 F\,/\,s \tag{15}$$

$$k_7 \cdot B_{(0)} \cdot F = 0.68 F\,/\,s \tag{16}$$

Figure A7   Variation of the concentration $B_{(0)}$ of the PBP, and of the rate constants of reaction 7. The parameters $B_{(0)}$ and k_7 strongly influence the fall of the receptor potential; k_{-7} only controls its tailing.

Thus, the enzymatic degradation contributes much more to the pheromone deactivation (26%) than in the redox model where only 1% of the adsorbed molecules were degraded directly. In the scavenger model this fraction would increase to 78% if $E_{(0)}$ is increased 10-fold, and decrease to 3.5% if $E_{(0)}$ is decreased to 1/10.

A further reduction of E has almost no effect on the deactivation and the fall of the receptor potential.

Variations of k_{10}, k_{-10} and k_{11} in the scavenger model do not affect the kinetics within the range of 20 s (not shown), as in the redox model.